New insights from Rheo-SANS

Michelle A. Calabrese and Norman J. Wagner[1]

Center for Neutron Science, Department of Chemical and Biomolecular Engineering, University of Delaware, Newark, DE 19716 USA

Abstract

Rheo-small angle neutron scattering (rheo-SANS) methods combine microstructural SANS measurements with an applied deformation field in order to measure flow-induced structures in complex fluids. Such methods enable a robust characterization of the microstructure and flow properties of surfactant wormlike micelle (WLM) solutions. The development of new sample environments now enables the flow-induced microstructure to be measured in the three planes of shear: the flow-vorticity (1-3), flow-gradient (1-2) and gradient-vorticity (2-3) planes. Advances in neutron collection and data analysis have improved the temporal resolution of time-dependent responses, significantly reducing the time required to perform such measurements. Theoretical advances in constitutive modeling and the stress-SANS rule now permit the development and testing of structure-property relationships. Such methodologies have allowed flow instabilities, such as shear and vorticity banding, and shear-induced structural transitions to be identified in WLM solutions. Additional sample environments have enabled the study of WLMs under extensional and Poiseuille flows, in addition to flows in microfluidic devices.

Keywords: SANS Rheo-SANS Wormlike Micelles Rheology Self-Assembly Surfactant Viscoelasticity

1. Introduction

Surfactant wormlike micelles (WLMs) and other soft materials undergo various deformations during production, processing, transportation, and use. While often used as a model system for studying polymers and polyelectrolytes [1], WLMs exhibit their own unique dynamics due to their 'living' nature, as they break and reform under shear. Topological changes such as branching are easily controlled by altering the solution temperature or concentration [2, 3, 4]. Due to their self-assembled nature and tunable flow properties, WLMs find applications as oil and energy recovery fluids, as well as consumer and household products. In such applications, the unique 'breaking' rheology leads to gel-like rest behavior which quickly transforms to liquid-like flow under an applied, tunable stress. Wormlike micelles are also commonly used for studying non-linear flow phenomena and flow instabilities such as shear banding [5, 6, 7]. These non-linear flow phenomena imply that the microstructure of WLMs is significantly different under flow than that at rest. Such flow-induced changes in microstructure may be beneficial, such as reducing the viscosity during the pouring of liquid detergents or transporting fluids while drilling oil and gas wells, or detrimental, such as the degradation of product stability during shipping. Thus, it is critical to measure the rheology and microstructure under both steady and dynamic non-linear deformations. Rheo-SANS methods present a unique opportunity to develop a qualitative and quantitative understanding of the relationships between the WLM microstructure and macroscopic flow properties. In this chapter, we review the current state-of-the-art methods in rheo-SANS, specifically applied to WLMs, and provide some key findings that should be of interest to practitioners and researchers alike working with WLMs. While space limitations restrict how much we can include given the breadth and historical richness of this topic, we refer the reader to recent reviews of rheo-SANS [8], WLM rheology [9], and WLM scattering [10, 11].

[1]Corresponding Author: wagnernj@udel.edu

2. Rheo-SANS sample environments

Rheo-SANS methods have been used to determine the flow-induced structure of a variety of soft materials since the 1980s [12]. The term 'rheo-SANS' often implies SANS measurements which are performed in either a concentric cylinder Couette or parallel plate geometry during an imposed shear deformation, which may or may not involve simultaneous rheological measurements. Rheo-SANS methods enable the material microstructure to be probed in the three shear planes, which are illustrated in Figure 1: the 1-3 (flow-vorticity or velocity-vorticity) plane, the 2-3 (gradient-vorticity or velocity gradient-vorticity) plane, and the 1-2 (flow-gradient or velocity-velocity gradient) plane. The projections of the material microstructure onto each shear plane may be measured using a variety of SANS sample environments. In addition to illustrating each of the three shear planes, Figure 1 shows a sample scattering pattern from each plane that results from shear-induced alignment [13]. While the schematic illustrates ellipsoidal particles aligned in the direction of the flow in each plane, this alignment and anisotropic scattering is also typical of WLM solutions. The current rheo-SANS sample environments are depicted in Figure 2, and additional details of the geometries and sample cells can be found below. When the rheometer configurations shown in Figure 2a are used for the 1-3 and 2-3 plane scattering experiments, simultaneous rheology is recorded throughout the duration of the SANS measurement [14]. Measurements in the flow-gradient (1-2) plane (Figure 2b) are much more difficult, and as such, are restricted to SANS measurements during flow without simultaneous rheology [15, 13].

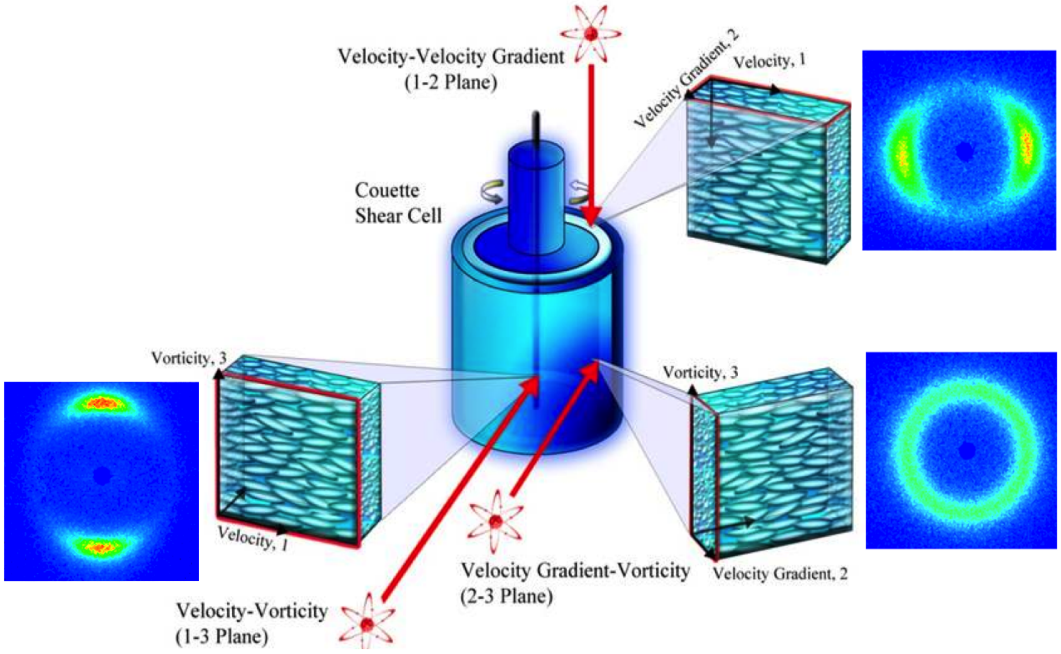

Figure 1: An illustration of the standard rheo-SANS sample environments displaying the three shear planes accessible by SANS. In order to access the 1-3 velocity-vorticity and 2-3 velocity gradient-vorticity planes, a rheometer is aligned in the neutron beam. To access the 1-2 velocity-velocity gradient plane, a new sample environment has been developed through a collaboration between the Institut Laue-Langevin (ILL, France), the National Institute of Standards and Technology Center for Neutron Research (NCNR, USA), and the University of Delaware (UD, USA). The schematic illustrates the direction of micellar alignment under shear flow in each plane, and sample scattering patterns are provided for each plane. Adapted from reference [16].

2.1. Rheo-SANS in the 1-3 (flow-vorticity) shear plane

Most rheo-SANS measurements of WLMs are performed in the 1-3 (flow-vorticity) shear plane (Figure 2a). Currently, these 1-3 plane experiments are performed using a rheometer outfitted with a quartz or titanium Couette cell centered in the neutron beam line [14]; however, initial experiments were performed using several custom-made Couette shearing apparati [12, 17, 18, 19, 20]. As WLMs tend to align in the flow direction upon shearing, the resulting increase in SANS anisotropy is symmetric along the vorticity direction (Figure 1). The resulting 2-D SANS pattern under shear is a convolution of the shear-induced

material microstructure across the Couette cell gap and an angle of alignment cannot be determined due to the symmetry imposed by the method. WLM solutions often exhibit spatially-dependent flow properties, such as shear banding [21], which cannot be resolved with these gap-averaged 1-3 plane measurements. However, spatially-resolved measurements along the vorticity direction may be performed using 1-3 plane rheo-SANS, which are useful in the detection of flow instabilities such as vorticity banding [22, 23]. Most experiments in the 1-3 plane use an Anton-Paar MCR stress-controlled rheometer with a concentric-cylinder Couette geometry (Figure 2) [14]. Additionally, a TA Instruments ARES-G2 strain-controlled rheometer with a concentric-cylinder Couette geometry is now available at the NCNR for 1-3 plane measurements. The rheo-SANS sample environment is available to users at several facilities worldwide, currently including the Institut Laue-Langevin (ILL, Grenoble, France), Laboratoire Leon Brillouin (Saclay, France), Paul Scherrer Institute (PSI, Villigen, Switzerland), Rutherford Appleton Laboratory (ISIS, Harwell Oxford, UK), University of Tokyo (Tokyo, Japan), Australian Nuclear Science and Technology Organisation (ANSTO, New South Wales, Australia), National Institute of Standards and Technology (NIST) Center for Neutron Research (NCNR, Gaithersburg, MD, USA), and Oak Ridge National Laboratory (Oak Ridge, TN, USA).

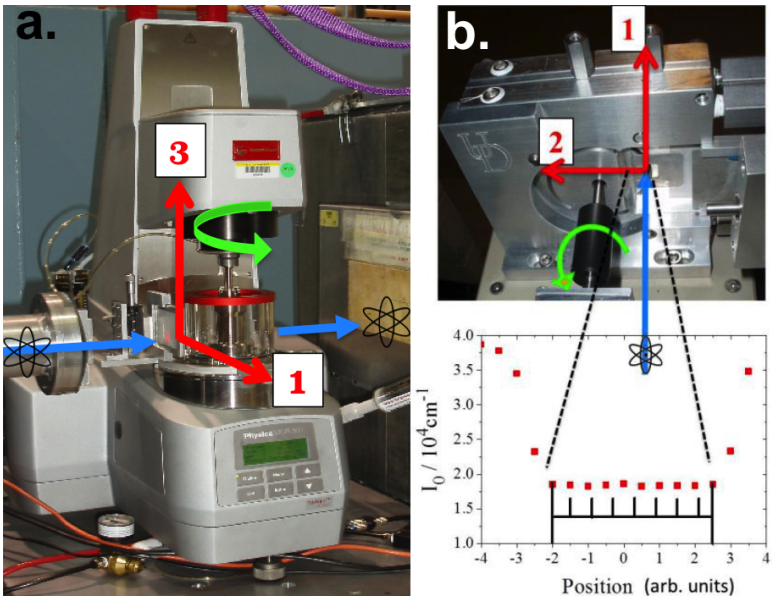

Figure 2: Current rheo-SANS instruments. The beam direction is represented by the blue arrows, the shear plane directions by the red arrows, and the rotation direction by the green arrows. (a) Anton-Paar MCR rheometer used at the NCNR aligned in the beam line for the 1-3 plane measurements, which also may be aligned for 2-3 plane measurements. (b) The 1-2 plane shear cell aligned in the beam for spatially-resolved measurements. (b) Reprinted with permission from reference [13].

2.2. Rheo-SANS in the 2-3 (gradient-vorticity) shear plane

Rheo-SANS experiments in the 2-3 (gradient-vorticity) plane probe the microstructure from the viewpoint along the flow direction. The same rheometer and Couette cell as in the 1-3 plane experiments is used; however, the configuration is altered so the Couette cell is tangential to the beam (Figure 1). Further, a thin vertical cadmium slit limits the scattering volume to the Couette cell gap. Ideally, the slit and rheometer are aligned such that the beam direction is parallel to the flow direction. In practice, these measurements include some curvature effects such that the scattering has a small component out of the 2-3 plane.

2.3. Flow-SANS in the 1-2 (flow-gradient) shear plane

To access the 1-2 (flow-gradient) plane with SANS methods, the Couette cell must be designed to lie horizontal with its rotation axis parallel to the beam. To accommodate such measurements, a sealed, short aspect ratio 1-2 plane shear cell was recently designed [15, 13], which can be seen in Figure 2b. This orientation enables obtaining spatially-resolved information across the Couette gap, which has proven useful in the detection of shear banding flow instabilities [24, 25, 26, 27, 28, 29]. The 1-2 shear cell is a short Couette (5mm path length) as described by Gurnon et al. [13]. The cell consists of a rotating inner

cylinder (R_1 = 25.5 mm) and an outer stationary cylinder (R_2 = 26.5 mm) such that the gap width is 1.0 mm, the resulting aspect ratio, Γ = L/H = 5 and the gap to radius ratio, ε = H/R = 0.039. Temperature control is maintained by a flow-through port within the cell that is connected to a water bath. A stepper motor is used to translate a cadmium beam aperture across the gap, providing spatial resolution. The 1-2 plane shear cell is currently available at the NCNR and the ILL.

2.4. Non-standard flows and geometries studied with SANS

While the term 'rheo-SANS' implies concentric cylinder Couette shear flow, other flows have been investigated using unique sample environments. These non-standard geometries have enabled extensional, channel, contraction-slit, rotating disk, and pipe flows of WLM solutions to be studied with SANS. Microfluidic devices at the ILL [30] and micro-flow-SANS cells at the NCNR have also been recently developed, where shear rates on the order of 10^5 have been accessed. While not used as extensively as rheo-SANS, these sample environments enable flow-structural relationships to be derived during complex flows. Further, some of the non-standard geometries require less volume than standard rheo-SANS experiments, allowing a wide range of soft matter systems to be studied.

Poiseuille flow is usually assumed for the analysis of extensional flows, laminar pipe flows, and channel flows. SANS studies of WLMs in extensional flows have used a cross-slot flow cell, where the center of the cross-slot forms a stagnation point of pure extension [31, 32]. These cross-slot flow cells are available at ISIS and the NCNR, where the aspect ratio may be altered in the NCNR design [32]. In these studies, spatially-resolved SANS measurements are performed at different positions along the flow cell. Poiseuille flow calculations are used to determine the velocity profile and average shear rates in the cell, to enable comparisons between the microstructural effects of shear and extensional flows. Other SANS Poiseuille-flow devices include planar flow cells [33, 34, 35], pipe flow apparati [36, 37, 38], and channel flow cells [39, 40]. Microstructural results from the laminar pipe flow regime (Poiseuille) have also been compared with the microstructures formed during turbulent flow [37, 38]. Similarly, spatially-resolved micellar alignment and instabilities formed by contraction-slit flow have been extensively studied in a recently designed cell [41, 42]. Finally, the shear flow of WLMs driven by rotating disks (i.e. parallel plates) has been examined in several designs [43, 18], such that angle between the beam and the shear gradient can be controlled.

3. Analysis of microstructural rearrangements using SANS

Wormlike micelles tend to show strong alignment in the flow direction during shear flow [8], as well as a variety of other flows, including extension [31], pipe flow [36, 37, 38], and contraction slit flows [41, 42]. Several metrics are commonly used to quantify these microstructural rearrangements. Early works compared differences in the absolute scattering intensity, $I(q)$, under flow in the 1-3 flow-vorticity plane with contour plots of the 2-D intensity [44, 45, 46, 47], or with sector-averages of $I(q)$ in the perpendicular (vorticity) and parallel (flow) directions, $I(q_\perp)$ and $I(q_\parallel)$, respectively [48, 49, 50, 51, 52]. An example anisotropic scattering pattern in the 1-3 plane can be seen in Figure 3a, where $I(q_\perp)$ and $I(q_\parallel)$ are compared to the static intensity in Figure 3b. Note that here, $q_\perp$ or q_ω correspond to the vorticity (3) direction, and $q_\parallel$ or q_v correspond to the flow (1) direction. Later, order parameters used in the analysis of liquid crystal microstructures were incorporated into the analysis of shear-induced WLM microstructures. These parameters quantify the measured microstructural rearrangements based on scattering anisotropy. The commonly used metrics include the $\overline{P_2}$ orientation parameter [53, 54, 55] and the scalar 'alignment factor,' A_f, [56, 15, 22, 57] with the angle of alignment of the primary eigenvector, ϕ_0. Note that in the case of 1-3 and 2-3 plane rheo-SANS, ϕ_0 cannot be measured due to the symmetry imposed by the method, whereas ϕ_0 can be determined in 1-2 plane measurements. In general, as the microstructure for a WLM can be described by a second order tensor formed by a dyadic product of an end-to-end vector, $\underline{Q}$, as $< \underline{Q}\,\underline{Q} >$, measurements in all three planes of flow are necessary to fully characterize the microstructure under flow [25]. As SANS probes microstructure on length scales from the nanometer to the micron (see Figure 3), the predominant source of flow-induced anisotropy in the SANS spectra is segmental alignment. As segmental alignment is also the primary source of elastic stress in the flowing WLM solution, and this elasticity can also be represented by $< \underline{Q}\,\underline{Q} >$, a formal 'stress-SANS' rule [25] can be derived for WLMs in direct analogy to the stress-optical rule [58].

The anisotropy parameters are calculated from the scattered intensity in the q^{-1} (rod-like segment) scattering regime; an example can be seen in Figure 3a, where the order parameter was calculated as $\overline{P_2}$ = 0.8. The rod-like scattering regime is usually chosen to focus on segmental alignment of WLMs. However, it is not uncommon for $\overline{P_2}$ or A_f to be calculated as a function of q-position [56]. A value of zero represents a system that is, on average, isotropic and non-aligned, whereas a value of one is the theoretical perfectly aligned state corresponding to a nematic order of thin, rigid rods. The scalar $\overline{P_2}$ orientation parameter is calculated by the integral:

$$\overline{P_2} = \int_0^{\pi} f(\theta) P_2(\theta) sin(\theta) \mathrm{d}\theta \tag{1}$$

where $f(\theta)$ is the projection of the normalized orientation distribution function (ODF) onto the shear plane (intensity distribution), and θ is the azimuthal angle with respect to the flow direction.

While the calculations are different, $\overline{P_2}$ is roughly equivalent to the alignment factor, defined as [56]:

$$A_f(q) = \frac{\int_0^{2\pi} I(q,\phi) \cos(2(\phi - \phi_0))\, \mathrm{d}\phi}{\int_0^{2\pi} I(q,\phi)\, \mathrm{d}\phi} \tag{2}$$

where I(q) is the intensity over a small fixed q-range and ϕ is the azimuthal angle and ϕ_0 is the azimuthal angle of maximum intensity. A general anisotropy parameter is also commonly estimated by the ratio of the perpendicular and parallel intensities from the 2-D SANS patterns; however, this method does not take the alignment angle or ODF into account.

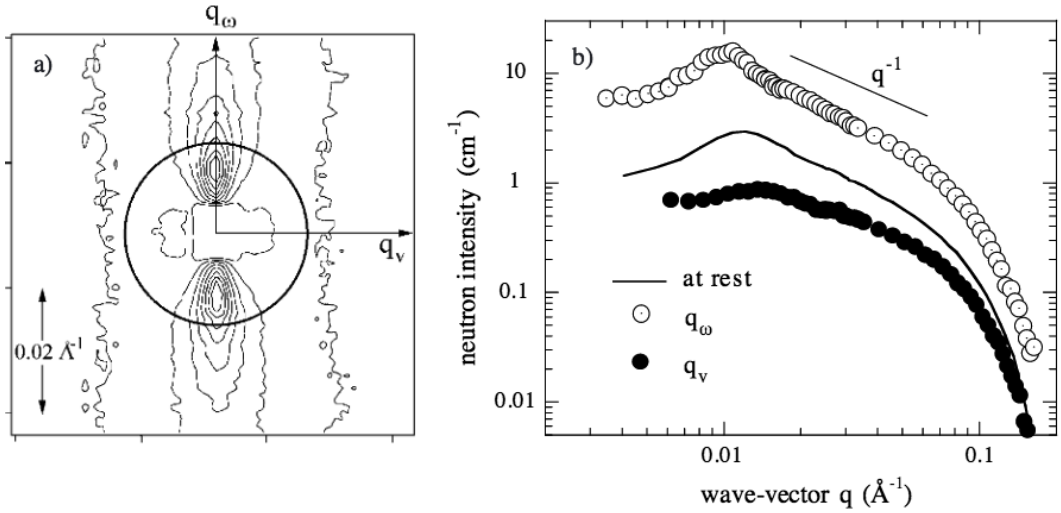

Figure 3: 1-3 plane intensity contour plot of the 2-D SANS pattern (L) and resulting SANS 1-D intensities in the perpendicular vorticity ($I(q_\perp)$) and parallel flow ($I(q_\parallel)$) directions (R, noted here as q_ω and q_v, respectively) for a shear thickening CTAT solution (ϕ = 0.26% wt) at $\dot{\gamma} = 188$ s^{-1}. (L) The 2-D SANS pattern under shear shows significant anisotropy along the vorticity-direction in a butterfly-type pattern, indicating strong alignment. (R) The 1-D averaged $I(q_\perp)$ is significantly larger than the intensity at rest or $I(q_\parallel)$. The interaction peak q-position in $I(q_\perp)$ shifts to lower q-values with increasing shear rate. Reprinted with permission from reference [59].

The aforementioned stress-SANS rule was developed to determine the polymeric stress from the alignment factor [25], based on the Giesekus-diffusion (G-D) model. Using the alignment factor and the azimuthal angle of maximum intensity, the stress-SANS rule is given by:

$$\tau_{12,p} = G_0 (C A_f)^{1/2} sin(2\phi_0) \tag{3}$$

$$N_{1,p} = 2 G_0 (C A_f)^{1/2} cos(2\phi_0) \tag{4}$$

where $\tau_{12,p}$ is the polymeric shear stress, $N_{1,p}$ is the polymeric first normal stress difference, G_0 is the plateau modulus and C is the stress-SANS coefficient, a constant determined on a per-system basis.

Several works have used the stress-SANS rule to successfully predict the polymeric stress when compared to the measured shear stress; however this relationship breaks down in the event of highly non-linear flows [25, 16, 26, 27]. While the stress-SANS coefficient, C, is a constant, a shear-rate dependent stress-SANS coefficient has shown promise in relating the alignment factor and stress in such non-linear flows [16]. A variety of other empirical relationships between the order parameter and shear rate or viscosity have been developed [60, 61], displaying power law and exponential dependences, respectively.

4. Summary of rheo-SANS systems and literature

Commonly studied WLM solutions using rheo-SANS include those of cetrimonium bromide (CTAB), cetrimonium tosylate (CTAT), and cetylpyridinium chloride (CPyCl), often with added counterions such as the hydrotropic salts sodium salicylate (NaSal) and sodium tosylate (NaTos), or simple salts such as sodium chloride (NaCl). Note that the addition of hydrotropic salt leads to micellar growth, while simple salts control the electrostatic interactions by screening or micellar charge by common-ion effects. Other common WLM systems include erucyl bis(hydroxyethyl)methylammonium chloride (EHAC), tetradecyltrimethylammoniumsalicylate (TTMASal), cationic surfactants with bromine groups (close structural similarity to CTAB), non-ionic surfactants and block copolymers. Many studies have examined the time-dependence of the microstructural responses, shear-induced structure formation (SIS), and flow instabilities including shear and vorticity banding and shear-induced phase separation (SIPS). The rheo-SANS literature has been summarized by solution strength in Table 1: dilute solutions, semi-dilute solutions, and concentrated solutions near the isotropic to nematic (I-N) transition. All solutions are in the isotropic phase at rest, and unless noted, are prepared in D_2O to reduce incoherent background scattering.

Table 1: Summary of rheo-SANS literature by concentration: dilute, semi-dilute, and concentrated near the isotropic to nematic (I-N) transition. Solutions with added salt are indicated by the (*) symbol, and mixed surfactant systems are indicated by the (†) symbol. Works that include non-standard geometries (extensional, planar, pipe flow, etc.) are designated by the (‡) symbol.

Surfactant	**Dilute**	**Semi-dilute**	**Near I-N**
CTAB	[57, 54]*, [41, 42]*‡	[48, 50, 19, 54]*, [61], [31]†‡ [39, 41]*‡, [47, 53]†	[25, 62, 24, 63, 64]
CPyCl	N/A	[22, 55, 23, 13, 16, 26, 27]*[32]*‡	[65, 66, 67, 68]*†
CTAT	[60]*, [69]†, [70, 59]	[4, 28, 29, 71]*†	N/A
EHAC	N/A	[15, 72, 73]*	N/A
TTMASal	[74, 46, 75]	N/A	N/A
Cationic+Br	[76], [19, 77, 78, 79, 57]*	[44, 45, 80, 76, 81], [48, 78, 79]*	N/A
Non-ionic	[82]	[61], [83]†, [31]†‡, [35]‡, [49]*, [52]*†	N/A
Industrial	[84]*, [40, 36, 37, 38]*‡	N/A	N/A
Other	N/A	[61], [47]† [34, 31]‡†, [48, 44, 50, 19]*, [39]*‡	[85, 86]†, [51]*

5. Steady shear, shear startup, and shear cessation studied via rheo-SANS

Rheo-SANS has been used most extensively to study WLMs under steady shear deformation. Initial experimentation primarily studied steady shear flows. Advances in instrumentation [15, 14, 13], detection [87, 27], and data processing [87, 29] have made time-resolved SANS techniques more widely available. These improvements have enabled the startup [75, 46, 27] and cessation of steady shear [45, 47, 27] to be examined in addition to time-dependent deformations such as large amplitude oscillatory shear (LAOS) [83, 55, 16, 29]. The following studies are presented in order of solution strength.

5.1. Dilute WLM solutions

In the initial development of flow devices for SANS, dilute WLM solutions were often used as model systems in both Couette [12, 19] and non-standard geometries [40, 36, 37]. Research has focused on shear thickening in these solutions, which is often observed when the surfactant concentration is approximately equal to or less than that of the overlap concentration to the semi-dilute regime, c^*. Above a critical shear rate, $\dot{\gamma}_c$, dilute solutions display a Newtonian-to-shear thickening transition, whereas solutions near c^* exhibit a shear thinning-to-shear thickening transition. The mechanism has been attributed to shear-induced structure (SIS) formation and micellar growth, which may also lead to elastic turbulence [21].

5.1.1. Common shear thickening WLM solutions - CTAT and CTAB

Berret and co-workers performed multiple rheo-SANS studies on dilute, shear thickening CTAT solutions [68, 59]. In these solutions, the overlap concentration occurs at $c^* \approx 0.5\%$ wt. Experiments were performed on two solutions below c^*: 0.26% wt [59] and 0.41% wt [68]. In both solutions, a cylindrical morphology was confirmed. At rest, an isotropic scattering ring was observed in the 2-D SANS pattern, which resulted in a correlation peak in the 1-D averaged SANS data. This correlation peak indicates strong interactions between the cationic WLMs, and can be seen in Figure 3b for the 0.26% wt solution. Each solution was then examined under shear, where an example anisotropic scattering pattern can be seen in Figure 3a for the 0.26% wt solution. At shear rates significantly above the critical shear rate, highly anisotropic, butterfly-like 2-D SANS patterns were observed in both solutions (Figure 3a). These 2-D SANS patterns indicated micellar alignment along the flow direction, which results in a strong anisotropy in the vorticity direction[2]. In the 0.26% wt solution, analysis of the orientation parameter ($\overline{P_2} \approx 0.8$ at $\dot{\gamma}$= 188 s^{-1}), suggested highly aligned, cylindrical micelles at these shear rates. In this regime above the critical shear rate, significantly different magnitudes were observed in the sector-averaged 1-D perpendicular and parallel intensities, where $I(q_\perp)$ increased and $I(q_\parallel)$ decreased with increasing shear rate in both solutions (Figure 3b). Here, the perpendicular direction refers to the vorticity (3) direction (q_ω in Figure 3), and the parallel direction refers to the flow (1) direction (q_v in Figure 3). Further, in the 0.26% wt solution, the q-position of the interaction peak decreased with increasing shear rate in the perpendicular direction, and increased in the parallel direction (Figure 3b).

In the 0.41% wt solution, two shear rates were examined: one below and one above the critical shear rate. Below the critical shear rate, anisotropic scattering was observed; however, a non-zero intensity contribution from the isotropic scattering ring was still evident. Above the critical shear rate, the scattering intensity was focused in the vorticity direction, similar to that seen in Figure 3a. Interestingly, a secondary q-peak appeared in the vorticity direction past the q-position of maximum intensity, at $q = 1.8q_{max}$. From the isotropic contribution to the scattering below the critical shear rate, the authors estimated the proportion, x, of the induced, shear aligned phase across the gap. The onset of shear thickening corresponded to the onset of SANS anisotropy ($x > 0$). Further, the maximum viscosity during shear thickening corresponded to a fully induced phase ($x = 1$). The authors concluded that shear thickening results from shear-induced micellar growth from short to entangled WLMs, and further postulated that worm-like aggregates may not be initially required for shear thickening. They also concluded that the shear thickening-to-shear thinning transition at high shear rates resulted from an alignment of the longer WLM chains.

Additional studies by Truong and Walker [60] examined the effect of added polymers polyethylene oxide (PEO) and hydroxypropylcellulose (HPC) on the shear thickening behavior of CTAT at the overlap concentration. While added PEO had little effect on the critical shear rate or the 1-3 plane alignment factor when compared to pure CTAT, added HPC increased $\dot{\gamma}_c$ significantly, thereby decreasing the alignment at equivalent shear rates. Despite such differences, an empirical, power-law relationship between the shear rate and 1-3 plane alignment factor was developed that described all solutions well. The alignment factor was also related to a critical scattering angle, q_{xo}, that is inversely related to the micellar persistence length in uncharged solutions [60]. Results indicated that the dependence of q_{xo} on A_f was independent of added polymer type or concentration. The authors concluded that the transition and growth of the aligned state is universal, and that the effects of the shear-induced structure dominate the effects of the added polymer.

[2]The reciprocal nature of scattering is such that the scattering intensity is a 90° rotation as compared to the real space structure.

Lastly, the impact of electrostatic interactions on the shear thickening transition was examined in CTAT at the overlap concentration with added NaCl [69]. Salt addition dampened the magnitude of the shear thickening transition and increased the critical shear rate. No shear thickening or SIS formation was observed when the salt concentration was greater than or equal to the surfactant concentration. While the added salt did not affect the micellar cross-sectional radius, r_{cs}, the overall micellar contour length, L_c, increased and the interaction peak in the 1-D SANS was mitigated with salt addition. Several ratios of NaCl to CTAT were examined using 1-3 plane rheo-SANS spanning shear rates before and during the shear thickening transition. Truong and Walker [69] found that normalizing the applied shear rate by the critical shear rate ($\dot{\gamma}/\dot{\gamma}_c$) created a master alignment curve for all systems studied. While added salt can affect the presence of the SIS, the results confirmed that flow alignment is directly related to the shear thickening transition and that the mechanism of the transition is system-independent.

Similar results have been observed in shear thickening solutions of CTAB and similar cationic surfactants [57]. Using 1-3 plane rheo-SANS and flow-birefringence measurements, Dehmoune et al. [57] studied the shear thickening transition in very dilute (0.1 % wt) solutions of CTAB (C_{16}TAB), C_{14}TAB and C_{18}TAB, with equimolar NaSal. In these solutions, the critical shear rate and micellar cross-sectional radius increased with length of the aliphatic surfactant chain. Results were divided into three regimes, based on the critical shear rate and the shear rate of highest viscosity, $\dot{\gamma}_m$: regime I ($\dot{\gamma} < \dot{\gamma}_c$), regime II ($\dot{\gamma}_c < \dot{\gamma} < \dot{\gamma}_m$), and regime III ($\dot{\gamma} > \dot{\gamma}_m$). In regime I, minimal anisotropy was observed in the CTAB and C_{14}TAB solutions, resulting in similar perpendicular and parallel intensities. Significantly higher anisotropy was observed in the C_{18}TAB solution. In regimes II and III, $I(q_\perp)$ was significantly greater than $I(q_\parallel)$ in all solutions due to micellar alignment in the flow-direction, in agreement with previous results [59]. The alignment factor was then compared to the birefringence results for each solution in the three regimes. While the alignment factor did not significantly change with shear in the C_{18}TAB solution, the CTAB and C_{14}TAB solutions showed qualitatively similar trends: low alignment in regime I, increasing alignment with applied shear rate in regime II, and nearly constant alignment in regime III. The alignment factor correlated strongly with the birefringence intensity, Δn, with little change in the extinction angle, indicating an increase in the proportion of the SIS with shear rate. These results further confirmed the link between shear thickening, SIS formation, and shear-induced anisotropy. Additional studies on C_{18}TAB/NaSal at the same concentration yielded similar results in regime III for the anisotropy ratio [78, 79]. However, the behavior of the C_{18}TAB/NaSal solution in regime II in these works [77, 78, 79] was similar to that of the CTAB and C_{14}TAB solutions from Dehmoune et al. [57], where the alignment increased with shear rate in this regime. Possible differences in sample preparation or temperature (which was not reported) resulted in slight differences in the 1-D SANS between the two C_{18}TAB solutions, which may account for the discrepancies.

Takeda et al. [54] examined three CTAB solutions: 0.16% wt (Newtonian-to-shear thickening), 0.33% wt (shear thinning-to-shear thickening), and 1.62% wt (shear thinning only) with added sodium tosylate. While Berret et al. [68] postulated that wormlike aggregates may not be required for shear thickening, Takeda et al. [54] systematically studied the transition from spherical to cylindrical micelles using static SANS and rheology, and confirmed that shear thickening only occurred in solutions of cylindrical micelles. Unlike previous studies, Takeda et al. [54] examined both the 1-3 plane and the 2-3 plane SANS microstructures. In the Newtonian-to-shear thickening solutions, isotropic scattering was observed at shear rates prior to shear thickening in both the 1-3 (radial) and 2-3 (tangential) planes. During the transition, the radial 2-D SANS patterns became more anisotropic with shear rate, and remained anisotropic in the shear thinning regime directly following the shear thickening regime. However, the shape of the anisotropic scattering pattern was ovular with a thick waist, as opposed to butterfly-like as seen in Figure 3a. As seen in previous studies [59, 57], $I(q_\perp)$ increased with shear rate, while $I(q_\parallel)$ decreased. The tangential 2-D SANS patterns were isotropic at all shear rates, indicating strong alignment in the flow direction. Similarly, in the shear thinning-to-shear thickening solutions, isotropic scattering was observed in the tangential direction at all shear rates. However, the scattering in the radial direction exhibited mild anisotropy even in the shear thinning regime. At the onset of shear thickening, strong butterfly-like anisotropy was observed in the radial direction. Finally, the shear thinning solution was investigated, and a large degree of anisotropy was observed in the thinning regime. Strong butterfly-like anisotropy was also observed that resembled that of the shear thinning-to-shear thickening solution. The differences in the shape of the 2-D anisotropy (ovular

vs. butterfly-like) between the systems suggest differences in the shear-induced structures and possibly the mechanism of alignment, which is consistent with differences in anisotropy seen between dilute and semi-dilute sheared systems in related works [77, 78, 79]. The authors concluded that the Newtonian-to-shear thickening transition resulted from micellar growth from short, rodlike micelles to worm-like chains, and further postulated that the shear thinning-to-shear thickening transition resulted from shear-induced growth which led to inter-micelle connectivity or branching.

5.1.2. Time-resolved experiments: startup and cessation of flow

Transient 1-3 plane rheo-SANS measurements were first used to study dilute, shear thickening solutions of trimethyltetradecylammonium salicylate (TTMASal) [46, 75]. As observed in other dilute solutions [77, 78, 79, 54], the shape of the anisotropy in these solutions was broad and ovular as opposed to butterfly-like, which was only observed at extremely high shear rates [80, 46, 75]. Münch et al. [75] proposed that the shear-induced structural transition resulted from a change in the proportion of short, rodlike, weakly aligned 'type I' micelles and longer, well-aligned 'type II' micelles in the solution. At various times following shear startup, the 1-3 plane scattering patterns were separated into contributions from type I or type II micelles, that resulted from distinct orientation distribution functions (ODFs). Münch et al. [75] observed that as the SIS formed in time, the contribution from type II micelles grew while the contribution from type I micelles decreased. The shape of the anisotropy from the type I micelles was broad and ovular, whereas butterfly-like patterns were seen from the type II micelles. The long times required for SIS formation help to explain the induction period observed during the shear thickening transition in rheological and SANS results [77, 78, 79, 57]. While the authors acknowledged that their two species model is too simple to fully describe the shear thickening transition, the results supported that micellar growth leads to shear thickening and SIS formation.

To investigate the stability of the SIS, Oda et al. [76] examined the time dependence of solutions of the gemini surfactant ethanediyl-1,2-bis(dodecyldimethylamonium bromide), also known as 12-2-12. Similar to previous works [59], the authors observed a shift in the peak q-position upon shear, but noted that this shift only occurs in solutions below c^*. Oda et al. [76] only observed anisotropy above a critical shear rate, as was observed by Takeda et al. [54] in Newtonian-to-shear thickening solutions. The authors then examined the 1-D SANS intensity in minute-long intervals after the cessation of flow. Whereas flow birefringence measurements decayed in approximately 10 s, the SANS anisotropy persisted on the order of 10^2 s, and changes in the overall SANS intensity were observed for times longer than 10^3 s. The authors concluded that aspects of the shear-induced structure are stable after the cessation of flow, and that one relaxation mechanism is not sufficient to describe the relaxation of these solutions.

A long relaxation mechanism after shear cessation was similarly described by Butler et al. [47] in solutions of cetyltrimethylammonium 3,5-dichlorobenzoate (CTA3,5ClBz) near the overlap concentration. The authors studied the different alignment and relaxation mechanisms in solutions with an added mixed counterion (MC) and homogenous counterion (HC). After shear startup in the HC system, the authors observed increases in the shear-induced anisotropy for up to 40 minutes. At high shear rates, an unexpected, two-stage alignment mechanism was observed. In the MC system, the transience was highly shear rate dependent, and the time-dependent anisotropy parameter at some shear rates displayed an overshoot similar in shape to stress overshoots observed upon shear startup [27]. While the HC system showed full structure relaxation within 10 minutes of shear cessation, the MC solution was still anisotropic after 100 minutes, suggesting a similar long-term stability of the SIS as observed by Oda et al. [76].

5.1.3. Summary - dilute solutions

Rheo-SANS studies on dilute WLM solutions have linked the shear thickening transition to shear-induced structure (SIS) formation, which results in anisotropic 1-3 plane SANS patterns under flow. Very dilute solutions display an ovular anisotropy, whereas solutions near the overlap concentration show butterfly-like anisotropy at high shear rates. The anisotropy results from the scattering from highly aligned cylindrical micelles in the flow-direction, which is supported by isotropic 2-3 plane patterns during shear thickening. Time-resolved experiments have shown that the steady state SIS is observed only after an induction time, which may be on the order of 10^3 s or more. With increasing shear rate in the shear thickening regime, $I(q_\perp)$ increases, $I(q_\parallel)$ decreases, and the peak q-position may shift to lower q-values. At shear rates above

the shear thickening transition, the order parameter remains at a maximum, indicating that the shear induced structure does not degrade. Upon shear cessation, the aspects of the SIS are stable and may persist for times on the order of 10^3 s.

5.2. Semi-dilute WLM solutions

Rheo-SANS studies of WLMs in the semi-dilute regime include concentrations above the overlap concentration but far below the isotropic-to-nematic transition on the phase diagram. Transitions between the dilute, semi-dilute, and concentrated regimes are often marked by a change in the dependence of characteristic length and time scales [2]. While the bounds of the semi-dilute regime are surfactant-specific, generally solutions ranging from 1% to 10% wt are considered semi-dilute. As concentrations in the semi-dilute regime may span an order of magnitude, a rich and varied flow behavior is expected across the regime, which can be well-characterized using rheo-SANS.

5.2.1. Shear thinning solutions

Similar to dilute solutions, semi-dilute WLM solutions show increasing in SANS anisotropy with increasing shear rate, illustrated in Figure 4 for a mildly branched WLM solution. This increase in anisotropy is pronounced in the 1-3 and 1-2 planes, whereas little change in the anisotropy is observed in the 2-3 plane. The 1-3 plane anisotropy becomes more butterfly-like with shear [39, 48, 45], and the ODF can be used to calculate theoretical intensity contours for comparison with experimental results. Förster et al. [61] measured the orientational ordering and distribution functions in a series of semi-dilute WLM solutions of different compositions, consisting of 1% to 10% wt PB-PEO polymer, CTAB or CPySal. Due to the nature of the surfactant blocks and concentration, the micellar properties varied greatly among the solutions; however, the authors reported that the shear-induced anisotropy for all solutions in the 1-3 plane was well-described by an Onsager ODF. Using a shift factor and the reduced shear viscosity, the viscosity showed an exponential dependence on the calculated order parameter, despite differences in WLM solution composition and concentration. Deviations from the exponential relationship were observed at high order parameters (high shear rates). A similar change in the order parameter scaling with viscosity in highly ordered solutions has been reported in recent works [28]. Studies on semi-dilute, shear thinning solutions of CTAB and added polymer were also well described by the Onsager ODF, and were equally well described by the Maier-Saupe ODF [53]. Both of these ODFs are commonly used to evaluate the orientation of WLM solutions under shear [56, 61, 53, 21].

5.2.2. Flow instabilities: Shear banding, vorticity banding, and shear-induced phase separation (SIPS)

Wormlike micelle solutions display a variety of flow instabilities such as shear banding. During shear banding, the flow exhibits spatial heterogeneities and organizes into macroscopic bands of high shear rate (low viscosity) and low shear rate (high viscosity). Shear banding may occur along the gradient direction of the flow, referred to as gradient shear banding, such that the high shear rate band forms near the inner Couette wall and the low shear rate band forms near the outer Couette wall. Shear banding may also occur in the vorticity direction, known as vorticity banding, where the bands organize along the vorticity direction as opposed to the gradient direction. Shear banding occurs in systems that have an underlying constitutive equation that is non-monotonic [88, 89, 90]; however, shear banding is also possible in solutions with monotonic constitutive equations [91]. While gradient shear banding has been more commonly studied in WLM systems using rheo-SANS methods [24, 25, 16, 26, 27, 28, 29], several works have identified vorticity banding using rheo-SANS [22, 23]. The rheological signatures of shear banding and relevant experimental techniques are detailed in a review by Manneville [92].

Shear banding has been verified in WLM solutions using a variety of experimental methods, including rheo-optical flow birefringence [7, 62], rheo-nuclear magnetic resonance (rheo-NMR) [93, 94], and rheo-particle image velocimetry (rheo-PIV) [95, 96]. Spatially-resolved flow-SANS measurements in the 1-2 plane are especially useful in detecting shear banding, as the spatially-dependent microstructure information enables the location of the shear band interface to be determined [24, 25, 16, 27, 28]. An example of the spatially-dependent microstructure and its dependence on dimensionless shear rate, or Weissenberg number (Wi), can be seen for a semi-dilute solution of CTAT and SDBS with added NaTos in Figure 4, as featured in Calabrese et al. [29]. Figure 4 illustrates the characteristic differences in the 2-D SANS

patterns for shear banding (region II) and non-shear banding (regions I and III) behavior. In the shear thinning regimes (regions I and III), the 1-2 plane anisotropy decreases gradually and continuously across the concentric-cylinder Couette cell gap, as expected for a shear thinning fluid in a Couette based on the gradually decreasing stress field with radius. Conversely, for the shear banding solution (region II), a large and often discontinuous change in alignment is observed with increasing gap position. The discontinuity in the rate of change of material alignment as a function of increasing gap position is evidence for the coexistence of a high 'alignment band' and low 'alignment band' that correspond to the high and low shear bands, respectively. Similar results for shear thinning and shear banding solutions can be seen in Helgeson et al. [24] for concentrated CTAB solutions. Therein, Helgeson et al. [25] measured a critical value of the alignment factor and alignment angle at the shear band interface of ϕ_0^*= 17° and A_f^* = 0.18, such that in the high shear band, $\phi_0 < \phi_0^*$ and $A_f > A_f^*$, while in the low shear band, $\phi_0 > \phi_0^*$ and $A_f < A_f^*$. Using these critical values as a guideline, along with the qualitative trends in the 2-D SANS anisotropy from 1-2 plane measurements, shear banding has been confirmed in a variety of other semi-dilute solutions [16, 26, 27, 28].

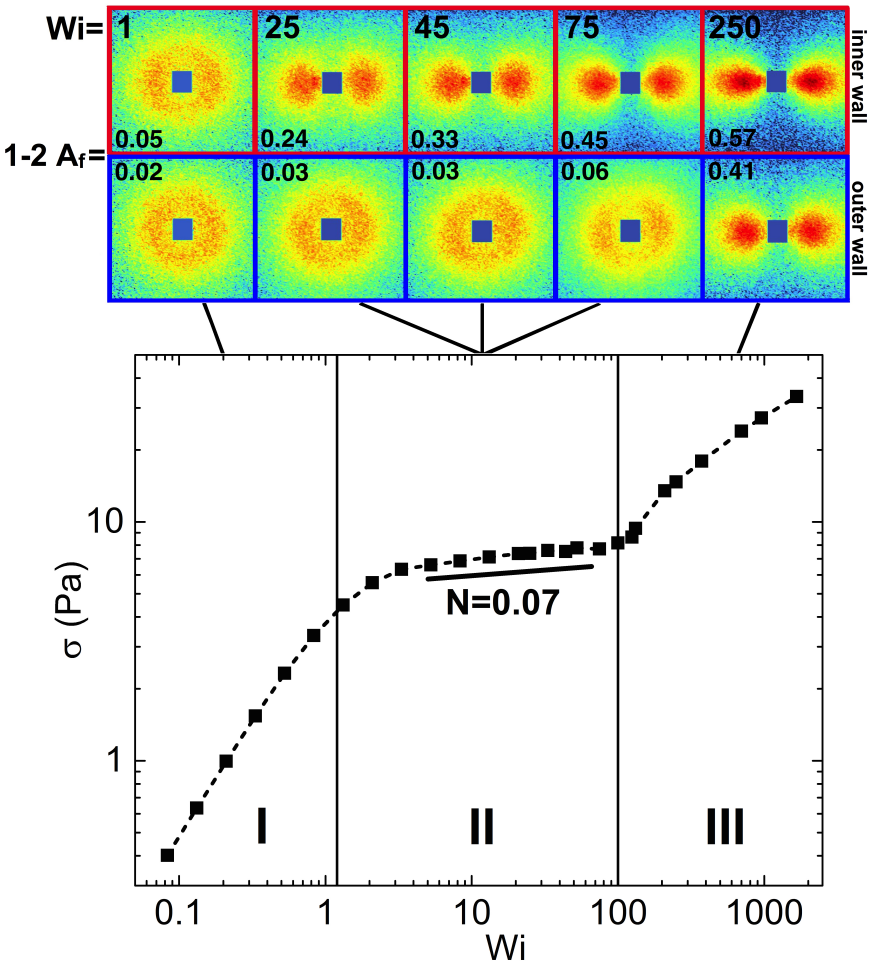

Figure 4: 1-2 plane 2-D SANS patterns as a function of gap position and dimensionless shear rate (Wi) for a shear banding, semi-dilute solution of 1.5% wt CTAT/SDBS with 0.05% wt NaTos, featured in reference [29]. The gradual and relatively minor decrease in anisotropy from the inner to outer wall, observed in regions I and III, is a signature of shear thinning and a continuous flow profile. The significant, discontinuous decrease in anisotropy across the gap in region II is a clear signature of shear banding.

One widely studied shear banding solution is CPyCl and NaSal in brine (6.0% wt) [55, 16, 26, 27]. In the shear banding regime, this system displays qualitatively similar behavior to that shown in region II of Figure 4, indicative of shear banding [16, 26]. Outside of the shear banding regime (regions I and III), shear thinning is confirmed by SANS measurements which show gradual changes in microstructure and anisotropy across the gap, similar to regions I and III in Figure 4. The critical values for the alignment factor and alignment angle set forth by Helgeson et al. [24] appear to apply to the semi-dilute regime, as the 1-2 plane SANS results for the 6.0% wt CPyCl/NaSal solution from Gurnon et al. [26] are in good

agreement.

In less concentrated solutions of CPyCl/NaSal (1.8% wt), both gradient and vorticity shear bands were identified using a variety of SANS techniques [22, 23]. Herle et al. [22] investigated an equimolar CPyCl/NaSal system using stress-controlled 1-3 plane rheo-SANS. In the shear thinning regime, the 1-3 plane SANS displayed a weak anisotropy. Above a critical applied shear stress, an oscillating shear rate response was observed, indicating an instability. Here, the measured SANS anisotropy was significantly larger and butterfly-like. The oscillating shear rate response was linked to clear and turbid alternating vorticity bands, which was confirmed using a high speed camera. Time-resolved 1-3 plane SANS experiments were then performed to determine the structure of each band. While the overall micelle radius did not change between bands, the material was significantly more aligned in the turbid band than in the clear band. The micelles in both bands, however, were significantly more aligned than those in the shear thinning regime. Mütze et al. [23] expanded upon this work using CPyCl and x-Sal at similar concentrations, where x refers to added counterions including lithium, sodium, potassium, magnesium and calcium. Here, the number of vorticity bands observed in each system was dependent on the applied shear stress, and the minimum concentration required for shear banding was dependent on the chemical nature of the counterion. Vorticity bands were only observed in equimolar solutions of surfactant and salt. Mütze et al. [23] showed that at applied stresses much above the critical stress, gradient shear bands only were observed, which corresponded with the alternating shear rate rheological response. However at intermediate stresses, vorticity bands or both vorticity and gradient shear bands were possible. The existence of simultaneous, alternating shear and vorticity bands was shown by a combination of rheology, laser transmittance measurements, high speed camera videos, and time-resolved 1-3 plane SANS measurements. As the shear rate signal oscillated at twice the frequency of the laser transmittance and microstructural SANS signal, the time dependence of the vorticity banding could be determined. The authors concluded that with increasing molar mass, the number of gradient shear bands increased, while the number of vorticity bands remained constant.

In contrast to the threadlike micelles, highly branched networked micelles such as erucyl bis (hydroxyethyl)methylammonium chloride (EHAC) exhibit a shear-induced phase separation (SIPS) that has been identified with rheo-SANS [15]. A combination of SANS measurements in the three shear planes along with rheo-optics and rheo-PIV measurements were used to characterize the phase separation of a 3% wt EHAC/4.1% wt NaSal solution. A distinct clear and turbid phase were detected above a critical shear rate. In the 1-3 and 1-2 planes below the critical shear rate, the observed anisotropy was consistent with weakly aligned, shear thinning micelles; nearly isotropic scattering was observed in the 2-3 plane. The 1-3 and 1-2 plane alignment factors at four gap positions were then compared above the critical shear rate. The magnitude of the gap-dependent alignment factor was similar to that observed in other semi-dilute, shear banding solutions [16, 26, 28, 29], and was considerably less than was observed in concentrated, non-phase separating micelles during shear banding. The alignment factor near the inner wall also exceeded the critical value determined by Helgeson et al. [24], and decreased across the gap in a manner consistent with shear banding. The authors concluded that the shear-induced banded structure was distinctly different than that of shear banding nematic-like micelles, and that the turbid phase was consistent with a flow-aligned, branched gel-like dense network microstructure coexisting with brine.

The proximity of the 3% wt EHAC/4.1% wt NaSal solution to the two-phase boundary on the phase diagram helps to explain the shear-induced transition to phase separation. The phase separation in this system is due to excessive branching and network formation coupled with ionic screening, and the SIPS has been attributed to shear-induced branch formation by Thareja et al. [97]. In EHAC solutions further from this boundary, SIPS does not occur, as shown by Liberatore et al. [72] for a 3% wt EHAC/13.7% wt NaSal solution. Here, scattering from the three shear planes was examined, where highly aligned micelles were observed at high shear rates. At intermediate shear rates, the 1-2 plane alignment factor and anisotropy decreased steadily and continuously across the gap, consistent with shear thinning as opposed to SIPS, as verified with rheology and PIV measurements. Despite differences in behavior between the two EHAC solutions, the 1-3 plane anisotropy and alignment factors were similar for both, which highlights the importance of the 1-2 plane spatially resolved measurements for the determination of flow instabilities. Salt addition has a strong effect on EHAC solutions, as well as the previously mentioned CPyCl solutions, in terms of the phase behavior, stability, and whether or not SIPS and shear banding will occur. Rheo-SANS

experiments in the 1-3 plane were also performed on similar EHAC solutions with added KCl [73] and the alignment results were qualitatively similar to those observed in the other two EHAC solutions. However, as the 1-3 plane measurements lack spatial resolution, no information about SIPS or shear banding could be elucidated.

5.2.3. Time-resolved experiments: startup and cessation of flow

In WLM solutions, the mechanism of shear band formation has been debated. Berret [98] proposed that upon shear startup, a nematic-like phase near the inner rotating cylinder nucleates and grows outward. However, transient rheo-PIV measurements by Hu and co-workers [95, 96] suggest that the wormlike chains disentangle upon startup and break, enter a long-lived metastable shear thinning state, and finally settle into shear bands, where the chains in the outer shear band re-entangle. Both works used a CPyCl/NaSal solution in brine; however Berret [98] studied a 12% wt solution, whereas Hu and co-workers used a 5.9% wt solution [95, 96]. López-Barrón et al. [27] used time-resolved SANS measurements in the 1-2 plane upon shear startup to confirm the mechanism of shear band formation in a similar CPyCl/NaSal solution (6% wt) [55, 16, 26]. To make precise measurements, López-Barrón et al. [27] used an acquisition trigger synched with the SANS instrument and 1-2 shear cell motor to acquire data immediately upon shear startup. SANS results were compared to time-resolved small angle light scattering (SALS) measurements during shear band formation. For the startup experiments, two shear rates were selected: one below the critical shear rate for the onset of shear banding and one in the shear banding regime. For the lower shear rate, a small stress overshoot was observed in the rheology, and both the stress and 1-2 plane alignment factor evolved steadily in time to steady state values. The steady state alignment factor and angle values were consistent with shear thinning as opposed to shear banding [24]. The stress-SANS rule was then used to calculate the shear stress and normal stress differences, which compared favorably to the measured values.

Significantly different behavior was observed for the startup of shear rates in the shear banding regime, where SANS measurements were taken near to the moving inner Couette cylinder (r/H = 0.2) and the outer stationary cylinder (r/H = 0.8). A large stress overshoot was observed in the rheology, which corresponded to nearly isotropic scattering. However, immediately following the stress overshoot, the scattering became highly anisotropic indicating strong shear alignment at both the inner and outer walls. During the course of the startup experiment, the material at the inner wall (high shear band) remained highly aligned and did not significantly change in structure. However, the material at the outer wall (low shear band) evolved from highly aligned to only weakly flow-aligned micelles. These results confirm the mechanism of shear banding presented by Hu and co-workers [95, 96] by showing that the micelles strongly align upon startup, and that the low shear band micelles re-entangle upon band formation to a nearly isotropic microstructure. On longer length scales, SALS measurements showed butterfly-like patterns, indicating density fluctuations and order on longer length scales. Once again, the stress-SANS rule was used to calculate the shear and normal stresses; however, the stress-SANS coefficient used was an order of magnitude higher than had been used in the homogeneous flow calculations. With the adjusted stress-SANS coefficient, the stresses were calculated prior to the onset of shear banding by using microstructure values from either band. After the onset of shear banding, only the calculated stresses from the high shear band were reasonable, confirming the breakdown of the stress-SANS rule for highly non-linear flows. This highly non-linear behavior was discussed within the context of shear-induced micellar breakage.

The relaxation of the shearing homogeneous and shear banded states were also probed. In the homogeneous state, both the stress and alignment factor relaxation were exponential, as predicted by the Maxwell model. In the shear banded state, however, the stress relaxation was fit to two exponential decays while the alignment factor was described by a single exponential decay after a lag time. A qualitatively similar decay of $\overline{P_2}$ was seen in reverse micelles, where a bi-exponential was used as opposed to a single exponential with a lag time [85]. The initial, extremely fast decay in stress corresponded to a disappearance of the butterfly-pattern in the SALS measurements and therefore, were associated with relaxation of the density fluctuations on the micron scale. During this relaxation period, no change or relaxation was observed in the alignment factor. Once the stress entered the second, slower relaxation process, the measured stress and alignment factor decayed commensurately. The combination of rheological, SALS and 1-2 plane SANS measurements therefore enabled the separation of relaxation processes and shear band formation mechanism to be determined. Additionally, relaxation experiments in the 1-3 plane in concentrated, reverse micelles [85]

support the 'disentangle, re-entangle' mechanism of shear band formation. Angelico et al. [85] observed that the relaxation to the isotropic state occurs gradually with no azimuthal angular dependence, and the relaxation is characterized by a continuous increase of the angular width. They noted that if the relaxation mechanism was instead nucleation and growth, the peaks should decay with constant width and an isotropic contribution to the scattering should increase in time, neither of which were observed.

5.2.4. Behavior of branched WLM solutions

While shear banding is common in linear WLM solutions, altering the WLM solution composition or temperature can result in morphological changes such as branching [2, 99, 28, 29] that may affect rheology and shear banding. These structural changes lower the zero-shear viscosity, η_0, of the solution by providing another mechanism for stress relaxation [100, 101]. Rheo-SANS methods in both the 1-3 and 1-2 planes in linear and branched WLMs have shown that branching may alter or eliminate the shear banding behavior of the solution [28, 29]. In these semi-dilute systems of CTAT and SDBS (1.5% wt), sodium tosylate (NaTos) was added as a hydrotropic salt to induce branching [2, 28]. Rheo-SANS results for a solution with mild branching (0.05% wt NaTos) are featured in Figure 4. In rheological measurements, the stress plateau increased in slope with increasing branching, indicating that shear banding was inhibited. This resulted in different shear-induced structures as a function of gap position when branched and unbranched solutions were compared [28, 29]. At high branching levels, 1-2 plane SANS and PIV measurements confirmed the absence of shear banding.

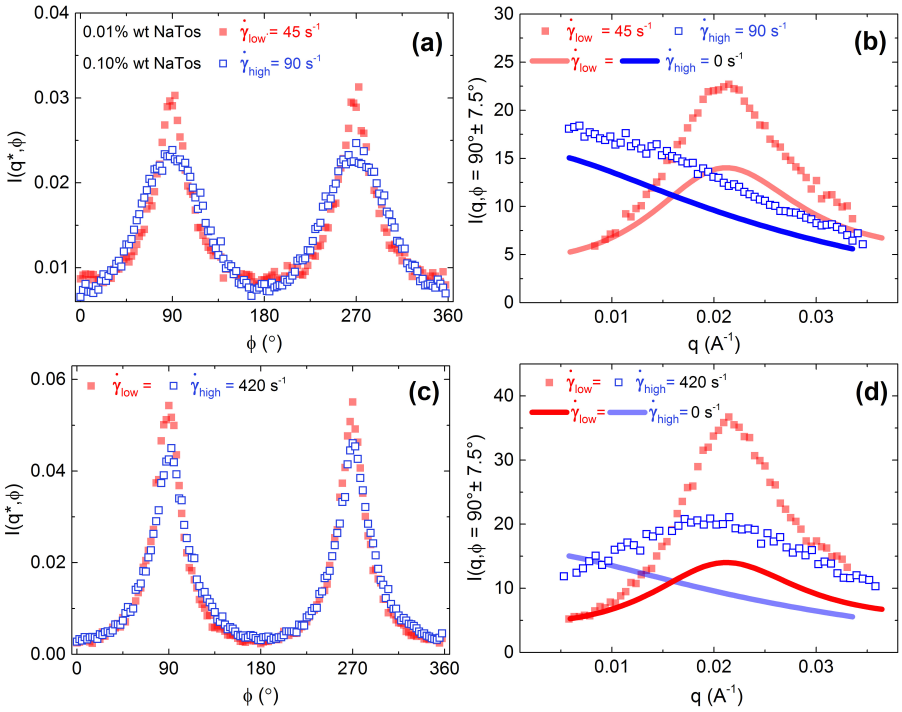

Figure 5: Orientation distribution function (L) and sector-averaged 1-D SANS in the anisotropy direction (R) for low and highly branched samples before (top) and after shear thickening (bottom). In a), for the same alignment factor, the ODF of the low branched sample is sharper than the highly branched sample, as a result of topological differences. b) The SANS structure for the branched sample under shear is nearly identical to the static branched structure (blue line). c) Both samples have the same alignment factor and nearly identical intensity distributions after shear thickening, but structural differences are evident in the 1-D SANS (d). In d), the 1-D scattering from the highly branched system is nearly identical to that of the low branched system (red line). In contrast, the structure for the low salt system under shear shows increased flow alignment but the correlation peak maintains its position with increasing rate. Reprinted with permission from [28]. Copyright 2015, The Society of Rheology.

Similar to the work of Förster et al. [61] and Nakamura and Shikata [53], the ODF of the branched and linear micelles under shear was examined in the 1-3 plane. While the Onsager and Maier-Saupe distributions described the orientation of these previous systems well, Calabrese et al. [28] found that the ODFs of the WLMs were significantly different between branching levels. With increasing branching, the ODFs under shear widened, reflecting the branched topology. Figure 5a shows the normalized intensity distributions for

both low and highly branched solutions. Clearly, topological differences affect the shape of the ODF (Figure 5b), leading to equal alignment factors despite different underlying ODFs. With increasing shear rate, the ODFs of the highly branched systems remained broader than that of the low branched counterparts, until a critical shear rate was surpassed. At this critical shear rate, a shear thickening structural transition occurred, which was verified by a change in the 1-D scattering. After the transition, the ODFs collapsed onto the same curve (Figure 5c) and similar 1-D SANS structures were observed between the branched and linear systems (Figure 5d), suggesting that shear-induced branch breakage was the source of the structural transition [28]. Further, this work emphasized that the ODF under flow contains critical information about the topology of sheared WLMs, which may have interesting implications for understanding branching effects in polymer rheology.

5.2.5. Summary

A wealth of rheo-SANS literature has focused on semi-dilute WLM solutions over a range of surfactants and compositions. Shear induces strong micellar alignment that may result in flow instabilities such as shear and vorticity banding, or for the case of highly-branched network micelles, shear-induced phase separation. This alignment is detectable using 1-3 plane SANS, where the gap averaged microstructure is measured, or using spatially-resolved 1-2 plane SANS, which can detect flow heterogeneities as a function of gap position. The 1-2 plane shear cell experiments enable gradient shear banding flow instabilities to be detected, which have shown to be mitigated by the introduction of branching. In the 1-3 plane, new experimental methods that combine light and neutron scattering with time resolution enable alternating shear and vorticity bands to be detected. Time-resolved 1-2 plane measurements have further advanced the study of flow instabilities, by helping to elucidate the mechanism of shear band formation. Shear-induced micelle breakage and branching are implicated as underlying mechanisms for the highly non-linear rheological behavior characteristic of these semi-dilute WLM solutions.

5.3. Concentrated WLM solutions near the I-N transition

Only a limited number of WLM solutions in the concentrated regime have been studied using rheo-SANS (Table 1). These systems undergo a shear-induced isotropic to nematic (I-N) transition, as at slightly higher concentrations, the equilibrium state is nematic. The shear-induced I-N transition drives shear banding, where the high shear band is para-nematic and the low shear band is primarily isotropic. This transition is believed to result from flow-concentration coupling, where the nematic band is of higher concentration than the isotropic band [66, 63]. This concentration-coupled shear banding distinguishes concentrated systems from semi-dilute systems, where the shear banding is not associated with concentration gradients [26].

5.3.1. 1-3 plane rheo-SANS

The first concentrated system to be extensively studied using rheo-SANS was CPyCl and hexanol in brine (30 - 38 % wt) [65, 67, 66, 68]. The solutions are nematic at rest when $\phi \geq 35.2$ % wt [65]; however, the 35.2 % wt solution aligns further under shear and is maximally ordered when $\overline{P_2} \approx 0.7$. In the 31 % wt solution, Roux et al. [66] observed that the 2-D SANS pattern under shear in the shear banding regime contained scattering elements of the isotropic pattern superimposed with elements of the nematic pattern. The superposition of these microstructures in the 1-3 plane SANS patterns was used as evidence of flow-concentration coupling [65, 68]. The authors noted that as the shear rate was increased, the q-position of the isotropic ring shifted to lower q-values, suggesting a lower concentration in the low shear band [65]. Using several 1-3 plane measurements across the shear banding regime, the authors estimated the proportion of the isotropic and nematic phases based on the 2-D isotropic and nematic contributions to the scattering. In shear banding WLMs, the proportion of material in the high and low shear bands is expected to increase linearly with shear rate [88, 102]; however, the results presented by Berret et al. [68] do not follow this simple scaling. Interestingly, when the shear rate was normalized by the stress, a linear relationship was seen between proportion of material in each band and shear rate. The calculated order parameter of the estimated nematic contribution remained constant in the two-phase region ($\overline{P_2} \approx 0.65$), leading the authors to conclude that only an increasing proportion of the nematic phase could lead to the observed increase in anisotropy with increasing shear rate [68]. During the time of these studies, spatially-resolved 1-2 plane measurements were not available to determine the band width dependence on the shear rate.

A similar methodology was employed in rheo-SANS measurements of $CPClO_3$ solutions (20% - 37% wt) in $NaClO_4$ [51], where the 37% wt sample was nematic at rest. Qualitatively similar results to those of Roux et al. [66] were obtained when the relative anisotropy of the nematic phase was calculated as a function of shear rate, which was again found to be non-linear. The authors also demonstrated that the critical shear rate for the onset of shear banding decreased with increasing concentration, as any increase in concentration moves the solution in question closer to the nematic phase boundary on the phase diagram. A final study was performed using 1-3 plane rheo-SANS with complementary flow-birefringence measurements on a concentrated CTAB solution (ϕ = 18% vol) [62], where the nematic phase was observed at $\phi \geq 19.5$ % volume. Again, a non-linear relationship was observed between shear rate and anisotropy. The proportion of the nematic phase calculated from the 2-D SANS was linear only at low shear rates. Further, the calculated percentage of nematic phase greatly deviated from the flow-birefringence measurements of the shear band width. It is worth noting that flow-birefringence measurements detect the width of the bright and dark phases, or width of the high and low shear bands. In the case of concentration coupling, a linear relationship may not be expected between band width and shear rate, as the concentration in each band may differ.

It must be noted for all three of these systems that the 2-D SANS patterns in the 1-3 plane represent a convolution of the microstructures in the two phases in space (across the gap). While the 1-3 plane measurements were the best available at the time, the simple assumption necessary to calculate the relative anisotropy from the 1-3 plane data in each of these cases was not sufficient to accurately determine the proportion of each phase. This is evidenced by the discrepancy between the flow-birefringence and 1-3 plane SANS results in the aforementioned CTAB solution. Additionally, later measurements using the 1-2 shear cell showed that the proportion of each phase *was* linearly dependent on the shear rate [25], as expected from theory. These measurements also showed that the order parameter in the nematic phase was not constant, as proposed by Berret et al. [68]. Instead, the alignment in the high shear rate band increased with shear rate, thus invalidating the previous assumptions used to calculate the band width from the 1-3 plane data. These 1-2 plane SANS measurements will be discussed further in the next section [25].

Time-resolved measurements in the 1-3 plane were also performed in concentrated, reverse micelle solutions of water and lecithin near the I-N transition [85, 86]. Unlike in typical 1-3 plane results, the time-resolved measurements showed that the angle of orientation was often non-zero and oscillated with regard to the applied strain for shear rates inside of the shear banding regime. Due to the symmetry of the 1-3 plane method, the authors explained that the average micellar orientation was driven by the flow that must fluctuate out of the shearing plane to obtain non-zero angles. The authors attributed these results to a tumbling instability and out-of-plane kayaking modes, which is consistent with theory for sheared, nematic liquid crystals. These results are also supported by 1-3 plane measurements in concentrated CPyCl/Hex (35.2% wt), where tumbling was also concluded [67]. While Berret et al. [67] did not use time-resolved measurements, they observed a thin isotropic scattering ring in the tumbling regime, which is consistent with a time-convolution of the tilted, out of plane microstructures observed by Angelico et al. [86]. Angelico et al. [86] also experimentally observed that the strain period was not dependent on shear rate, in line with theory. While the authors could not rule out vortices in the high shear band or an unstable band interface as the source of the fluctuations, they postulated that the observed time-evolutions of the order parameter and angle represented a periodic transition between in-plane tumbling and out-of-plane kayaking, which sustained the unstable motion of the nematic director.

5.3.2. 1-2 plane shear cell determination of flow-concentration coupling

In order to determine characteristics of shear banding and non-shear banding systems, Helgeson and co-workers performed 1-2 plane measurements on concentrated CTAB solutions (15% - 21% wt) [24, 25]. These 1-2 plane measurements are performed with spatial resolution, such that different positions across the Couette shear cell gap may be examined. Two CTAB solutions were compared to show the differences in the shear-induced structures as a function of gap position in shear banding (16.7% wt, 32 °C) and shear thinning (15.6% wt, 30 °C) solutions [24]. Steady shear rheology and rheo-PIV measurements confirmed the shear thinning and shear banding behavior. The 1-2 plane SANS measurements were performed at five gap positions and five shear rates for each solution, in its respective shear thinning or shear banding regime. The 2-D SANS results are visually similar to those observed in semi-dilute solutions [16, 26, 27, 28] and seen in Figure 4: a large, discontinuous decrease in the anisotropy from the inner to outer wall is

indicative of shear banding, whereas a continuous and relatively minor change in anisotropy across the gap is indicative of shear thinning. In the shear banding solution, the high shear band material became more nematic-like with increasing shear rate, and the low shear band material also increased slightly in alignment. However, in the shear thinning solution, even the most highly aligned state clearly exhibited an isotropic ring despite measurable alignment, confirming the absence of shear banding.

The alignment factor and alignment angle were calculated as a function of gap position for each solution. The location of the shear band interface was then determined from rheo-PIV measurements, enabling a critical alignment factor, A_f^*, and alignment angle, ϕ_0^*, to be determined [24]. At the shear band interface, the critical alignment factor was A_f^* = 0.18 and the critical angle was ϕ_0^*= 17°. These critical values appear to be independent of surfactant and concentration [16, 26, 29]. Not surprisingly, the alignment factors for the shear thinning solution did not exceed the critical alignment factor required for shear banding, and only two measurements contained an angle less than the critical angle [24]. An additional study was conducted on the shear banding solution using 1-2 plane SANS, rheo-PIV, and flow-birefringence [25]. It was in this work that the stress-SANS rule given by Equation 3 was derived, based on the Giesekus-diffusion model. By combining the 1-2 plane measurements with rheo-PIV, Helgeson et al. [25] confirmed a linear relationship between shear rate and the proportion of material in each shear band, as predicted by theory [102].

5.3.3. 1-2 plane USANS verification of flow-concentration coupling

To directly measure and confirm flow-concentration coupling in concentrated shear banding solutions, additional 1-2 plane measurements were performed by Helgeson et al. [63] using transmission measurements by ultra small angle neutron scattering (USANS) on the shear banding CTAB solution (16.7% wt, ϕ = 0.196 by volume) [63]. In small angle neutron scattering experiments, the transmission of the surfactant solution can be directly related to its volume fraction by:

$$T = exp[-t(\Delta\sigma_{s12}\phi + \Sigma_a')] \tag{5}$$

where ϕ is the volume fraction, t is the sample thickness, $\Delta\sigma_{s12}$ is the difference in the incoherent scattering cross section between scattering objects and the surrounding medium, and Σ_a' is the incoherent scattering cross section.

As the low-q scattering of WLM solutions is known to increase under shear, an accurate transmission measurement is not currently possible using typical 1-2 plane SANS methods. USANS accesses much smaller length scales, enabling the increase in low-q scattering to be separated from the material transmission. In a flow-concentration coupled system, the transmission in the shear banding regime should be the lowest at the inner wall (high shear band) and highest at the outer wall (low shear band), indicating a higher concentration in the high shear band than in the low shear band. Integration of the concentration profile across the gap is used to validate the method, as the average surfactant concentration is independent of shear rate by conservation of mass.

Transmission measurements were performed in the 1-2 shear cell at five gap positions, both at rest and at five shear rates [63]. A narrow slit was used to access the different gap positions, such that the method is known as scanning narrow aperture flow-USANS (SNAFUSANS). The transmission as a function of gap position and shear rate can be seen in Figure 6a. As expected, the transmission of the sample at rest was independent of gap position. The sample transmission at shear rates prior to and beyond the shear banding regime was also independent of gap position, as expected for solutions of uniform concentration (Figure 6a). However, at the shear rates measured within the shear banding regime (denoted by color in Figure 6a), the transmission steadily increased as a function of gap position, with an average transmission equal to the transmission at rest. In Figure 6b, the concentration at each gap position for each shear rate was then calculated based on the transmission results. As seen in Figure 6b, at the shear rate where the greatest concentration change was seen, a volume fraction difference of $\Delta\phi \approx 0.07$ was observed between the inner and outer walls [63]. Combined with rheo-SANS and flow-PIV, these results enabled constructing the first non-equilibrium state diagram for concentrated WLMs exhibiting shear banding [24]. While still under development, the SNAFUSANS technique enabled a direct measurement of the WLM transmission, and therefore concentration, under shear for the first time, helping to confirm flow-concentration coupling

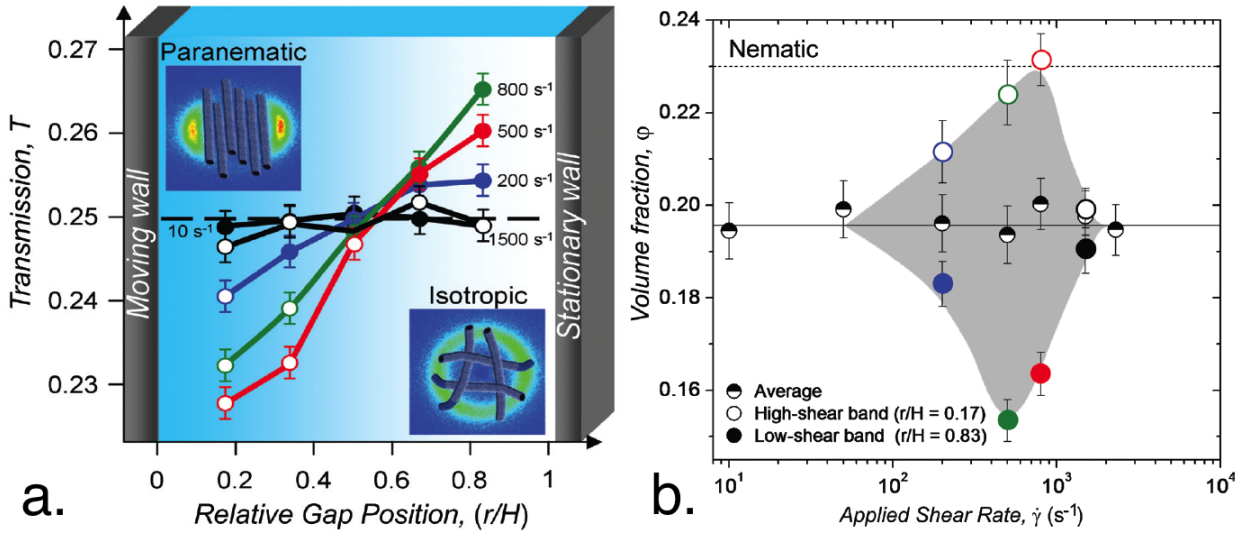

Figure 6: SNAFUSANS transmission measurements and resulting concentration differences during shear banding in 16.7% wt CTAB. a) The transmission measurements at five gap positions and five shear rates. Outside of the banding regime ($\dot{\gamma}$=10 s^{-1}, $\dot{\gamma}$=1500 s^{-1}), the transmission is independent of gap position. At the three shear rates in the banding regime, the transmission steadily increases as a function of gap position. b) Calculated volume fraction as a function of gap position and shear rate. At the shear rates outside of the banding regime, the concentration is constant across the gap. Within the banding regime, the concentration is highest near the inner wall (high shear band) and lowest at the outer wall (low shear band), indicating concentration-coupled shear banding. Reprinted from reference [64].

in concentrated shear banding systems. A follow-up study was conducted on a semi-dilute, shear banding solution of CPyCl/NaSal [26], used in several previously mentioned works [55, 16, 27]. As this solution is semi-dilute (ϕ = 0.066 vol) and far from the isotropic to nematic transition, concentration-coupled shear banding is not expected. The same SNAFUSANS method was performed on this solution. As expected, no evidence of concentration-coupled shear banding was observed and the measured transmission was not correlated to the gap position [26].

5.3.4. Summary

Few concentrated wormlike micellar solutions near the isotropic-to-nematic transition have been studied using rheo-SANS methods. Due to the proximity of the solutions at rest to the I-N transition, applying shear induced an I-N transition, where the critical shear rate for the onset of the transition decreased with increasing concentration and proximity to the phase boundary. These solutions exhibit concentration-coupled shear banding during the I-N transition, where the high shear band is more concentrated than the low shear band. While several works calculated the shear band width based on 1-3 plane measurements alone, 1-2 plane measurements were essential to accurately determine the band width. Finally, direct SNAFUSANS measurements of the spatially-dependent transmission were able to confirm flow-concentration coupled shear banding in these solutions.

6. Large amplitude oscillatory shear (LAOS) Rheo-SANS

The natural extension for rheo-SANS investigations into WLM rheology is to move from steady and step transient deformations to time-periodic measurements in the nonlinear regime, such as large amplitude oscillatory shear (LAOS). In LAOS, the applied strain is sinusoidal and the applied strain rate is co-sinusoidal, as seen in Figure 7a. This allows the separation of the elastic and viscous contributions to the stress response of the WLM by systematically varying the frequency and amplitude of the applied deformation. At sufficiently small strain amplitudes, the resulting stress response is sinusoidal in time (linear viscoelastic regime), where classical elastic, viscous and viscoelastic responses can be seen in Figure 7a. The stress response of a purely viscous (Newtonian) fluid is in phase with the applied strain rate, $\dot{\gamma}(t)$, and the response of a pure elastic (Hookean) solid is in phase with the applied strain, $\gamma(t)$ (Figure 7). In the deformation domain (Figure 7b), this translates to a straight line in the elastic projection of the 3-D

Lissajous-Bowditch diagram (top) for an elastic solid, and a straight line in the viscous projection (bottom) for a viscous fluid. A viscoelastic fluid displays an elliptical response. Reviews of experimental methods and analysis for LAOS provide detailed information [103, 104].

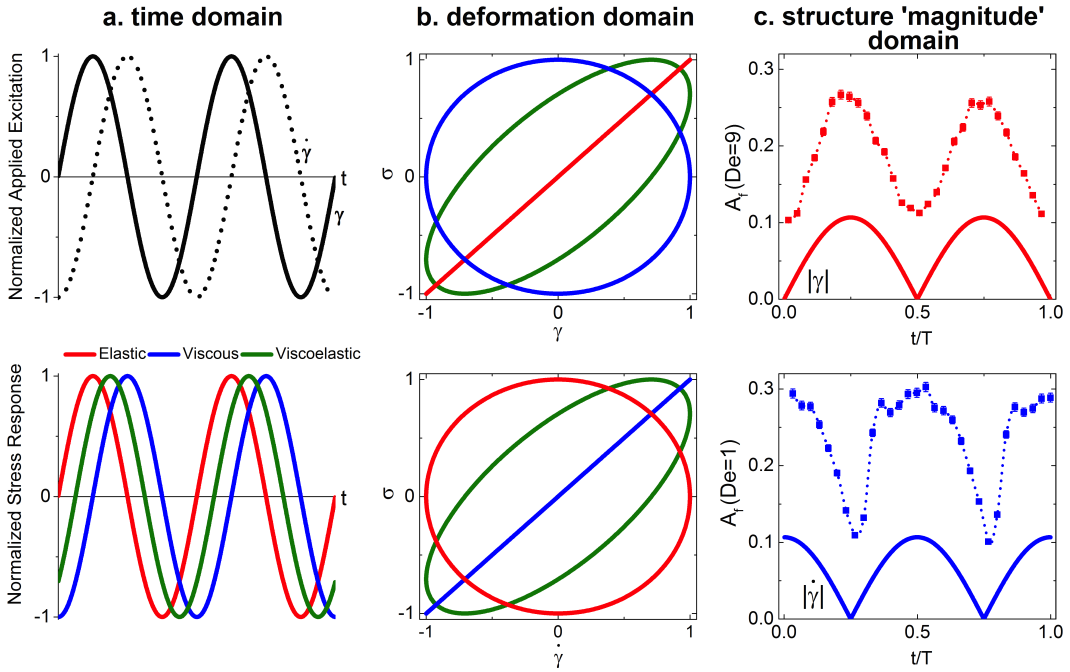

Figure 7: Large amplitude oscillatory shear (LAOS) and analysis. a) The applied strain and strain rate are sinusoidal and co-sinusoidal in time (top), and the resulting linear regime stress responses in time (bottom). A response in phase with the strain is a classical elastic response, and with the rate is a viscous response; phase shifted responses are viscoelastic. b) Elastic (top) and viscous (bottom) Lissajous-Bowditch curves of the linear stress responses, where the stress is analyzed in terms of the strain and the strain rate. The linear responses represent classical elastic (top) and viscous (bottom) behaviors. c) Microstructure or alignment factor responses that display elastic (top) and viscous (bottom) behavior through the oscillation. In each case, the alignment factor closely follows the phase and shape of the *magnitude* of the applied deformation, as A_f is a positive scalar quantity. In this WLM solution, the A_f response is elastic at high De and viscous at low De for the same maximum shear rate, as is expected.

LAOS responses can be categorized by the dimensionless groups applicable to the solution. The Deborah number ($De = \tau_R\omega$) and Weissenberg number ($Wi = \tau_R\dot{\gamma}$) are the dimensionless frequency and shear rate that characterize the applied oscillation, respectively, where ω is the applied angular frequency of the oscillation and τ_R is the material relaxation time. Under LAOS, the stress response is time-periodic, but no longer sinusoidal. However, aspects of this analysis may still be used to interpret LAOS microstructural responses, as seen in Figure 7c. Here, at a high Deborah number (top), the alignment factor of the WLM solution throughout the oscillation is in phase with the magnitude of the applied strain and has a similar shape, indicating elastic-like behavior. Conversely, at a much lower Deborah number (bottom), the alignment factor phase and shape are similar to the magnitude of the applied strain rate, indicating fluid-like behavior. The ideas presented in Figure 7b and 7c have been used along with other methods to interpret the stress and microstructure response of WLMs under LAOS, which will be discussed below.

6.1. WLM solutions - CPyCl, CTAT/SDBS, PB-PEO block copolymers

Rheo-SANS analysis of wormlike micelles under LAOS is limited. These WLM solutions include the two previously mentioned semi-dilute solutions of 6 % wt CPyCl/NaSal in brine [55, 16] and the 1.5% wt CTAT/SDBS solution with 0.05% wt NaTos [29], along with semi-dilute WLM solutions composed of 50-50 PB-PEO block copolymer constituents, ranging from 0.5% to 2.0% wt. In all of these works, the alignment factor or $\overline{P_2}$ order parameter was examined as a function of time during the LAOS oscillation and related back to the rheological stress response and applied deformation. Results were also compared to the steady shear case to relate the dynamic and steady WLM microstructures.

6.2. 1-3 plane rheo-SANS LAOS measurements

Rogers et al. [55] examined a 6 % wt CPyCl solution using 1-3 plane rheo-SANS to elucidate the relationship between the time-dependent rheological stress and micellar orientation $\overline{P_2}$. The authors examined several frequency (De) and shear rate (Wi) domains. Under steady shear for $Wi < 1$, the stress-orientation relationship was found to be quadratic, as predicted by the Giesekus model. In the low frequency and low rate amplitude regime ($De << 1$, $Wi < 1$), the authors expected, and confirmed, the same quadratic stress-orientation relationship. Conversely, in the low frequency and high rate amplitude regime ($De << 1$, $Wi = 5.7$), a complex relationship between the stress and $\overline{P_2}$ was observed. At decreasing shear rates, a linear relationship between stress and orientation was observed that mirrored the steady shear limit, indicating viscous flow (as discussed in Figure 7); however, the overall stress-orientation relationship could not be described by one function. Interestingly, the authors show that the dependence of the stress and $\overline{P_2}$ on the shear rate contains similar shapes and features, further indicating shear rate-dependent behavior, which has been confirmed in other WLM solutions under LAOS [71]. In the high frequency regime ($De > 1$), the observed stress responses of the solution were elliptical and could be described by a single-mode Maxwell model. At $Wi = 5.7$ for frequencies where $De > 1$, the orientation parameter was linearly dependent on the applied strain for much of the oscillation indicating an elastic strain-dependent response (Figure 7), unlike the viscous response observed at lower Deborah numbers.

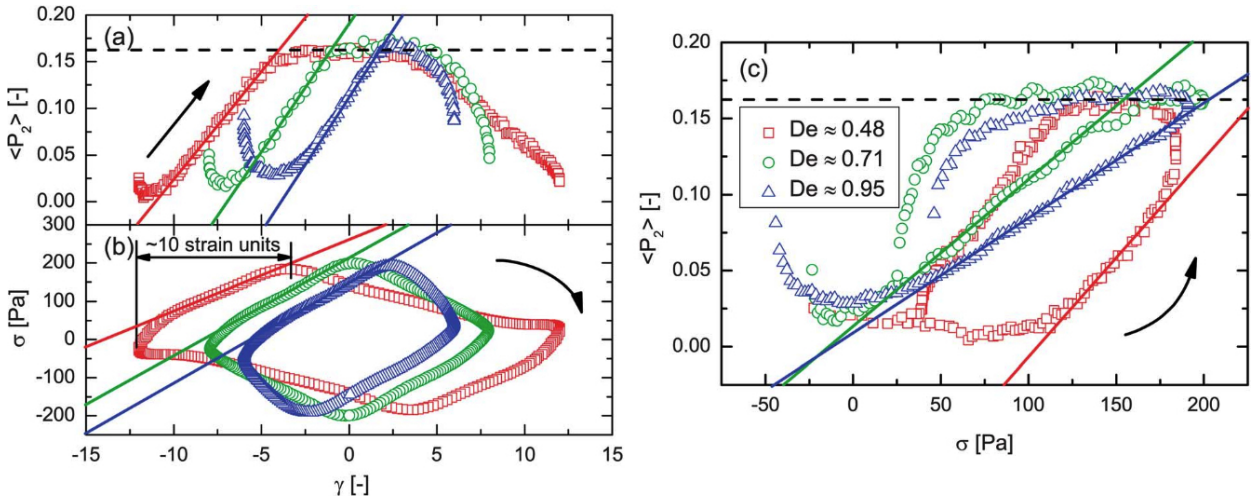

Figure 8: Order parameter (a) and stress (b) dependence on the strain, which both show linear behavior during portions of the LAOS cycle. The resulting stress-orientation relationship (c) also shows a linear relationship through portions of the cycle, indicative of elastic behavior and static yielding after 10 strain units, as shown in (b). Reprinted with permission from reference [55].

Lastly, an intermediate frequency range was examined ($0.5 \leq De \leq 1$) at $Wi = 5.7$, shown in Figure 8. A linear relationship was observed between $\overline{P_2}$ and the strain (Figure 8a), the stress and strain (Figure 8b), and the stress and orientation (Figure 8c) during portions of the oscillation, indicating elastic behavior. While the elastic Lissajous-Bowditch projections shown in Figure 8b are more complicated than the example shown in Figure 7b, the authors used the same analysis to explain the elastic behavior during the linear regions of the projections. As this elastic phenomenon occurred over ten strain units in each LAOS condition (Figure 8b), the authors attributed the behavior to static yielding. Higher strains resulted in viscous flow. They also observed 'over-orientation' directly following the yield point, where the LAOS order parameter was greater than that observed under steady shear. Based on the additional microstructural information gained by simultaneously measuring the segmental alignment and the shear stress, the authors concluded that: in the low shear rate regime, the material response is primarily rate-dependent; in the intermediate regime, the response is primarily strain-dependent; and in the high frequency regime, the response is Maxwellian. Rogers et al. [55] acknowledge that the 1-3 plane approach is limited by the inability to calculate an angle of orientation or determine spatial heterogeneities. The authors note that the solution in question is predicted to shear band under LAOS at these conditions [105] and use this in their interpretation. However, the same solution under similar LAOS conditions was shown not to shear band by Gurnon et al. [16] using 1-2 plane SANS, which will be addressed below. A similar analysis of

the frequency-dependent phenomena during LAOS was reported by Lonetti et al. [83] in PB-PEO block-copolymer WLMs, where the authors used a Fourier decomposition to analyze the order parameter and stress. As was seen by Rogers et al. [55], with increasing frequency, the solution behavior transitioned from fluid-like to elastic-like, whereas elastic to viscous transitions were observed with increasing shear rate.

6.3. 1-2 plane shear cell examinations of shear banding under LAOS

The majority of rheo-SANS experimental work on shear banding has focused on shear banding under steady shear flow and shear startup [24, 25, 26, 27]; however, shear banding and related flow instabilities have been predicted under LAOS [91, 105, 106, 107]. Adams and Olmsted [91] and Zhou et al. [105] have adapted constitutive models to identify Deborah number and Weissenberg number conditions for transient or steady state banding in concentric-cylinder Couette flow during LAOS. Other works have predicted shear banding or similar instabilities under LAOS by showing that a material may act simultaneously as a fluid and elastic solid during the cycle, depending on the gap position [106, 107]. Until recently [29], experimental verification of shear banding under LAOS was limited to rheo-PIV measurements in a cone-and-plate geometry [108, 109, 110, 111]. Dimitriou et al. [111] measured WLMs under LAOS, and in these studies, shear banding was concluded at the onset of non-linearity ($De < 1, Wi < 1$).

The model predictions of Adams and Olmsted [91] and Zhou et al. [105] assumed concentric-cylinder Couette flow, thus 1-2 plane shear cell measurements of WLMs under LAOS provide a more useful comparison with these theoretical results than the cone and plate measurements. Recent experimental work by Gurnon et al. [16] examined the same CPyCl/NaSal solution under LAOS as was examined by Rogers et al. [55], using spatially-resolved 1-2 plane SANS as opposed to 1-3 plane measurements. Two of the conditions explored had maximum shear rates during the oscillatory cycle that exhibited shear banding under steady shear (Wi =1.2, 2.3), which was confirmed with 1-2 plane steady shear measurements. Of these two conditions, one condition was not predicted to shear band under LAOS, while the other was on the border of the shear thinning and shear banding regimes [105]. Interestingly, the non-shear banding condition under steady shear ($Wi = 23$, region III) was well within the predicted shear banding regime under LAOS (De =2.3, Wi =23).

Surprisingly, Gurnon et al. [16] did not observe shear banding at any condition, but rather were able to access metastable homogeneous states conceptually predicted by the constitutive equation. In the condition predicted to show LAOS shear banding, the alignment factor was greater than the critical value for shear banding [24] at nearly every time point within the oscillation at both positions. The changes in alignment between the inner and outer wall were minor, indicative of shear thinning in region III. In the other two conditions, the alignment factor was always below the critical condition throughout the oscillation, confirming the absence of shear banding. The stress-SANS rule was also used to reconstruct the stress from the alignment factor in each condition. The stress reconstruction yielded favorable results to the measured stress for the majority of the oscillation cycle at low Weissenberg numbers; however, the stress reconstruction at the highest Weissenberg number showed significant deviations. Consistent with the results for steady shear at the corresponding maximum dynamic shear rate, a shear-rate dependent stress-SANS coefficient that was an order of magnitude larger than calculated at low Wi was required to give reasonable results. Again, complementary rheo-light scattering results demonstrated longer length scale fluctuations were evident at the highest stress states, which corresponded to length scales not probed by SANS. Gurnon et al. [16] concluded that LAOS deformation enabled the exploration of metastable states of homogeneous flow that were inaccessible under steady shear where shear banding occurs. Recent modeling work by Germann et al. [112] connects much of the observed behavior under LAOS to a model that explicitly includes shear-induced micellar breakage.

Calabrese et al. [29] examined LAOS shear banding near the end of the shear banding regime (region II into region III) for a branched, semi-dilute CTAT/SDBS system. The flow curve of this solution indicated shear banding up to $Wi = 100$ and was similar to that produced by the Vasquez-Cook-McKinley (VCM) model parameters in the work of Zhou et al. [105]. Therefore, the conditions where shear banding under LAOS was predicted were expected to be experimentally verified in this system. Steady shear 1-2 plane measurements were performed at eight shear rates to verify the shear banding regime. New time-resolved data analysis and processing techniques were then used for the LAOS measurements to significantly enhance the data resolution [71]. Seven LAOS conditions were then examined at shear rates near the end

of the shear banding regime and into region III (Wi = 64 to 113). In all but one of these conditions, the solution exhibited shear banding at the equivalent shear rate under steady shear deformation. Two unique mechanisms of shear banding under LAOS were identified. In LAOS cycles at low frequencies ($De < 0.3$), the shear banding resembled that of the steady shear case. Calabrese et al. [29] attributed the similarities to the long LAOS cycle, which allowed the material to fully relax through the oscillation to achieve its steady state microstructure and alignment. At intermediate frequencies ($0.3 < De < 0.6$), a metastable form of shear banding was reported, where the same 'over-orientation' seen by Rogers et al. [55] was observed when the LAOS alignment was compared to the steady shear alignment. The authors showed that at these conditions, the faster oscillation period led to incomplete material relaxation during the oscillation cycle, thereby trapping the outer shear band in a state of over-orientation. However, the oscillation period in these cycles was still long enough to allow for partial relaxation and shear band formation. At higher frequencies ($De > 0.6$), the fast oscillation cycle prevented material relaxation during the course of the oscillation, yielding an over-oriented, non-shear banded state at all gap positions. In total, shear banding was observed in four of the seven conditions, in excellent agreement with the VCM model predictions [105]. The results confirmed that shear banding under steady shear is required, but may not result in, LAOS shear banding, and that over-orientation may occur with or without shear banding.

6.4. Summary

While few studies have examined the microstructure of WLMs under LAOS, advances have been made using both 1-3 plane and spatially-resolved 1-2 plane rheo-SANS. As LAOS experiments must be repeated over many cycles to achieve proper statistics, triggering and time-stamping acquisition methods have been recently improved to reduce acquisition time [71]. The 1-3 plane rheo-SANS experiments are less time consuming due to the wider slit aperture, and yield interesting structural-flow relationships [55]. However, the nature of 1-3 plane SANS excludes the study of shear banding and other spatially-dependent flows, as the WLM microstructure is averaged across the gap in the 1-3 plane experiments. Using the 1-2 plane shear cell on shear banding WLMs provides key spatial information, which has enabled shear banding under LAOS to be experimentally verified in WLMs in Couette flow for the first time [29]. Importantly, rheo-SANS measurements enable critically examining structure-property relationships under dynamic conditions and states that are not accessible under steady shear. While some conflicting results between experiment [16] and theory exist [105], advances in constitutive equations that account for micellar breakage and reformation dynamics under shear flow promise to capture the dynamic coupling between microstructure and flow-induced structure, and its dependence on both WLM topology and processing conditions.

7. Results from non-standard flow cells

Several works have compared results from rheo-SANS experiments in the Couette geometry to other geometries, such as pipe flow (laminar and turbulent) [34], contraction-slit flow [41, 42], extensional flow [31, 32], and others. In the majority of these non-standard geometries, a similar anisotropy was observed under flow as seen in concentric cylinder Couette flow: broad, ovular anisotropy for dilute, rodlike solutions and butterfly-like anisotropy for semi-dilute, wormlike solutions. Similar differences in the parallel and perpendicular intensities were also observed [40, 36]. Solutions that exhibited butterfly-like anisotropy in laminar flows showed a transition to the broad ovular anisotropy in turbulent flows [37, 38]. This result is indicative of micellar breakage at high Reynolds number, and a return to short, rodlike micelles. At very high Reynolds numbers, the solutions became highly turbulent and returned to the isotropic state, as indicated by overlaying parallel and perpendicular intensities [40].

In the extensional flow and contraction-slit flow experiments, spatially resolved measurements were taken at a variety of positions along the flow field [31, 42]. Penfold et al. [31] studied a mixed micellar system of CTAB and $C_{16}E_6$ in a cross-slot extensional flow cell. The authors noted that significant alignment was achieved at much lower flow rates under extensional flow than under shear flow, and that at high shear rates, the anisotropy decreased due to the introduction of turbulent flow. The spatially-resolved 2-D SANS patterns from the cross-slot flow cell can be seen in Figure 9, which illustrates the level of spatial detail afforded by these measurements. The micellar alignment and angle are highly dependent on position

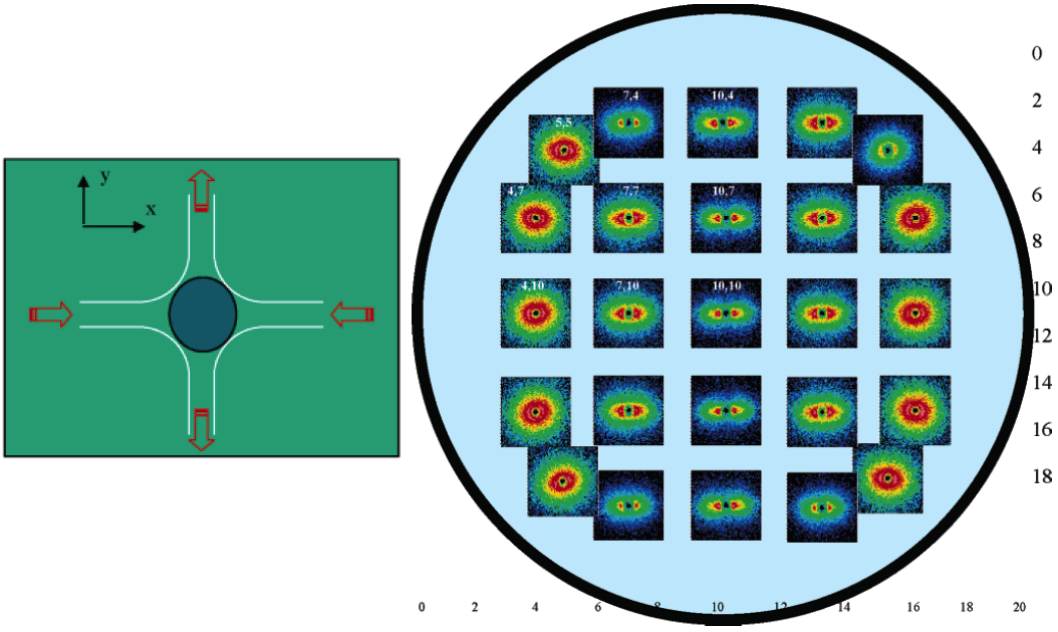

Figure 9: 2-D anisotropic scattering patterns (R) of extensional flow experiments, mapped across the cross-slot cell aperture (illustrated, L). The WLMs at the center stagnation point (10, 10) show the highest degree of ordering, consistent with strong extensional deformation at this position. Further from the stagnation point, the micelles become considerably less aligned, and the measurable alignment angle can be used to map the flow field. Reprinted with permission from [31]. Copyright 2006 American Chemical Society.

within the cell aperture, where the strongest alignment is seen at the center stagnation point (10, 10), which corresponds to pure extension. Further, as WLMs strongly align in the flow direction, the spatially-resolved results can be used to map the flow field, which was also done by Lutz-Bueno et al. [42] for CTAB solutions in contraction-slit flow.

8. Outlook

This brief overview of rheo-SANS studies demonstrates some of the valuable insights gained about the broad range of shear-induced microstructural changes coupled with, and responsible for, the nonlinear steady and dynamic rheology of wormlike micellar systems. As with polymers, entangled WLM solutions exhibit strong flow-alignment, resulting in shear thinning and a positive first normal stress difference. However, shear-induced topological changes manifest a much richer flow behavior, including shear-induced growth leading to shear induced structure (SIS) and shear thickening, shear-induced breakage leading to shear banding (SB), shear-induced branching leading to shear induced phase separation (SIPS), and shear-induced phase transitions coupled with concentration gradients. Throughout, rheo-SANS provides critical and unique structural information about micellar orientation, concentration, and state-of-aggregation on length scales of direct relevance to the macroscopic rheology. Importantly, this plethora of system microstructural responses to an imposed shear flow often drive instabilities, the simplest of which, stable shear banding, can be resolved by spatiotemporal resolution afforded by recent advances in 1-2 plane sample environments. Coupling rheology with SANS and allied methods such as particle image velocimetry and flow visualization is critical for mapping the local kinematics as well as the local microstructure in such structured flows. Advancing this to include more complex flows such as extensions, contractions and expansions will be invaluable for tailoring WLM solutions for applications. Work to date establishes many qualitative and quantitative structure-property relationships, but the wealth of chemistries and commensurate WLM topologies merits much future work and suggests new discoveries await.

Advances in our understanding of polymer rheology and constitutive equation modeling by methods such as flow-birefringence were promoted by development of quantitative stress-optical rules. Advances in constitutive equation modeling that can capture not only the elastic stresses of entropic nature, but also topological changes including branching, breakage, and micellar growth will be required for developing ro-

bust stress-SANS rules. Non-linear coupling with the flow kinematics in rheologically relevant geometries can be expected to lead to a wealth of instabilities of mechanical and thermodynamic nature, especially when shearing solutions with composition in proximity to a phase transition. While shear banding can find utility for some applications, for others, suppressing shear banding and related instabilities may be critical. Thus, research that identifies the underlying mechanism of nonlinear coupling can be used to control WLM rheology and ultimately, such instabilities. Engineering WLM solutions for specific applications will benefit from robust constitutive models that capture the wealth of WLM physical behaviors afforded by their self-assembled nature, and which are validated for accuracy in predicting both macroscopic rheology and microscopic structure in shear and more complex flows, such as those afforded by the advanced SANS sample environments illustrated in this chapter.

9. Acknowledgement

The authors acknowledge the support of the National Institute of Standards and Technology, U.S. Department of Commerce, and the Institut Laue-Langevin in Grenoble, France in providing the neutron research facilities used in this work. This manuscript was prepared under cooperative agreement 70NANB12H239 from NIST, U.S. Department of Commerce. The statements, findings, conclusions and recommendations are those of the author(s) and do not necessarily reflect the view of NIST or the U.S. Department of Commerce.

References

[1] Magid, L. "The surfactant-polyelectrolyte analogy," The Journal of Physical Chemistry B 1998;102(21):4064–4074.

[2] Schubert, B.A., Kaler, E.W., Wagner, N.J. "The microstructure and rheology of mixed cationic/anionic wormlike micelles," Langmuir 2003;19(10):4079–4089.

[3] Koshy, P., Aswal, V., Venkatesh, M., Hassan, P. "Unusual scaling in the rheology of branched wormlike micelles formed by cetyltrimethylammonium bromide and sodium oleate," The Journal of Physical Chemistry B 2011;115(37):10817–10825.

[4] Rogers, S.A., Calabrese, M.A., Wagner, N.J. "Rheology of branched wormlike micelles," Current Opinion in Colloid & Interface Science 2014;.

[5] Spenley, N., Cates, M., McLeish, T. "Nonlinear rheology of wormlike micelles," Physical Review Letters 1993;71:939.

[6] Berret, J.F., Roux, D.C., Porte, G. "Isotropic-to-nematic transition in wormlike micelles under shear," Journal de Physique II 1994;4(8):1261–1279.

[7] Makhloufi, R., Decruppe, J., Ait-Ali, A., Cressely, R. "Rheo-optical study of worm-like micelles undergoing a shear banding flow," Europhysics Letters 1995;32(3):253.

[8] Eberle, A.P., Porcar, L. "Flow-SANS and rheo-SANS applied to soft matter," Current Opinion in Colloid & Interface Science 2012;17(1):33–43.

[9] Cates, M.E., Fielding, S.M. Giant micelles: properties and applications; vol. 140 of *Surfactant science series*; chap. Theoretical Rheology of Giant Micelles CRC Press; 2007, p. 109–161.

[10] Pedersen, J., Cannavacciuolo, L., Schurtenberger, P. Giant micelles: properties and applications; vol. 140 of *Surfactant science series*; chap. Scattering from Wormlike Micelles CRC Press; 2007, p. 179–222.

[11] Walker, L.M. "Scattering from polymer-like micelles," Current Opinion in Colloid & Interface Science 2009;14(6):451–454.

[12] Lindner, P., Oberthür, R. "Apparatus for the investigation of liquid systems in a shear gradient by small angle neutron scattering (SANS)," Revue de Physique Appliquée 1984;19(9):759–763.

[13] Gurnon, A.K., Godfrin, P.D., Wagner, N.J., Eberle, A.P., Butler, P., Porcar, L. "Measuring material microstructure under flow using 1-2 plane flow-small angle neutron scattering," Journal of Visualized Experiments 2014;(84):e51068–e51068.

[14] Porcar, L., Pozzo, D., Langenbucher, G., Moyer, J., Butler, P. "Rheo-small-angle neutron scattering at the National Institute of Standards and Technology Center for Neutron Research," Review of Scientific Instruments 2011;82(8):083902.

[15] Liberatore, M.W., Nettesheim, F., Wagner, N.J., Porcar, L. "Spatially resolved small-angle neutron scattering in the 1-2 plane: A study of shear-induced phase-separating wormlike micelles," Physical Review E 2006;73(2):020504.

[16] Gurnon, A., Lopez-Barron, C., Eberle, A., Porcar, L., Wagner, N. "Spatiotemporal stress and structure evolution in dynamically sheared polymer-like micellar solutions," Soft Matter 2014;10(16):2889–2898.

[17] Cummins, P., Staples, E., Millen, B., Penfold, J. "A couette shear flow cell for small-angle neutron scattering studies," Measurement Science and Technology 1990;1(2):179.

[18] Kalus, J., Neubauer, G., Schmelzer, U. "A new shear apparatus for small angle neutron scattering (SANS) measurements," Review of Scientific Instruments 1990;61(11):3384–3389.

[19] Straty, G., Muzny, C., Butler, B., Lin, M., Slawecki, T., Glinka, C., et al. "In situ rheometric shearing apparatus at the NIST Center for Neutron Research," Nuclear Instruments and Methods in Physics Research Section A: Accelerators, Spectrometers, Detectors and Associated Equipment 1998;408(2):511–517.

[20] Porcar, L., Hamilton, W., Butler, P., Warr, G. "A vapor barrier Couette shear cell for small angle neutron scattering measurements," Review of Scientific Instruments 2002;73(6):2345–2354.

[21] Lerouge, S., Berret, J.F. Shear-induced transitions and instabilities in surfactant wormlike micelles In: Polymer Characterization. Springer; 2010, p. 1–71.

[22] Herle, V., Kohlbrecher, J., Pfister, B., Fischer, P., Windhab, E.J. "Alternating vorticity bands in a solution of wormlike micelles," Physical Review Letters 2007;99(15):158302.

[23] Mütze, A., Heunemann, P., Fischer, P. "On the appearance of vorticity and gradient shear bands in wormlike micellar solutions of different CPCl/salt systems," Journal of Rheology (1978-present) 2014;58(6):1647–1672.

[24] Helgeson, M., Reichert, M., Hu, Y., Wagner, N. "Relating shear banding, structure, and phase behavior in wormlike micellar solutions," Soft Matter 2009a;5(20):3858–3869.

[25] Helgeson, M., Vasquez, P., Kaler, E., Wagner, N. "Rheology and spatially resolved structure of cetyltrimethylammonium bromide wormlike micelles through the shear banding transition," Journal of Rheology 2009b;53(3):727–756.

[26] Gurnon, A.K., Lopez-Barron, C., Wasbrough, M.J., Porcar, L., Wagner, N.J. "Spatially resolved concentration and segmental flow alignment in a shear-banding solution of polymer-like micelles," ACS Macro Letters 2014;3(3):276–280.

[27] López-Barrón, C.R., Gurnon, A.K., Eberle, A.P., Porcar, L., Wagner, N.J. "Microstructural evolution of a model, shear-banding micellar solution during shear startup and cessation," Physical Review E 2014;89(4):042301.

[28] Calabrese, M.A., Rogers, S.A., Murphy, R.P., Wagner, N.J. "The rheology and microstructure of branched micelles under shear," Journal of Rheology 2015;59(5).

[29] Calabrese, M.A., Rogers, S.A., Porcar, L., Wagner, N.J. "Understanding steady and dynamic shear banding in a branched wormlike micellar solution," submitted to Journal of Rheology 2015;.

[30] Lopez, C.G., Watanabe, T., Martel, A., Porcar, L., Cabral, J.T. "Microfluidic-sans: flow processing of complex fluids," Scientific reports 2015;5.

[31] Penfold, J., Staples, E., Tucker, I., Carroll, P., Clayton, I., Cowan, J., et al. "Elongational flow induced ordering in surfactant micelles and mesophases," The Journal of Physical Chemistry B 2006;110(2):1073–1082.

[32] McAllister, R., Weigandt, K.M. "Extensional-flow sans of wormlike micelles," NIST Center for Neutron Research: Accomplishments and Opportunities 2015;:48.

[33] Baker, S.M., Smith, G., Pynn, R., Butler, P., Hayter, J., Hamilton, W., et al. "Shear cell for the study of liquid-solid interfaces by neutron scattering," Review of Scientific Instruments 1994;65(2):412–416.

[34] Hamilton, W., Butler, P., Hayter, J.B., Magid, L., Kreke, P. "Over the horizon SANS: Measurements on near-surface poiseuille shear-induced ordering of dilute solutions of threadlike micelles," Physica B: Condensed Matter 1996;221(1):309–319.

[35] Cloke, V.M., Higgins, J.S., Phoon, C.L., Richardson, S.M., King, S.M., Done, R., et al. "Poiseuille geometry shear flow apparatus for small-angle scattering experiments," Review of Scientific Instruments 1996;67(9):3158–3163.

[36] Bewersdorff, H., Dohmann, J., Langowski, J., Lindner, P., Maack, A., Oberthür, R., et al. "SANS- and LS-studies on drag-reducing surfactant solutions," Physica B: Condensed Matter 1989;156:508–511.

[37] Lindner, P., Bewersdorff, H., Heen, R., Sittart, P., Thiel, H., Langowski, J., et al. Drag-reducing surfactant solutions in laminar and turbulent flow investigated by small-angle neutron scattering and light scattering In: Trends in Colloid and Interface Science IV. Springer; 1990, p. 107–112.

[38] Lindner, P. "Small angle neutron scattering studies of liquid systems in nonequilibrium," Physica A: Statistical Mechanics and its Applications 1991;174(1):74–93.

[39] Hayter, J.B., Penfold, J. "Use of viscous shear alignment to study anisotropic micellar structure by small-angle neutron scattering," The Journal of Physical Chemistry 1984;88(20):4589–4593.

[40] Bewersdorff, H.W., Frings, B., Lindner, P., Oberthür, R. "The conformation of drag reducing micelles from small-angle-neutron-scattering experiments," Rheologica Acta 1986;25(6):642–646.

[41] Lutz-Bueno, V., Kohlbrecher, J., Fischer, P. "Shear thickening, temporal shear oscillations, and degradation of dilute equimolar ctab/nasal wormlike solutions," Rheologica Acta 2013;52(4):297–312.

[42] Lutz-Bueno, V., Kohlbrecher, J., Fischer, P. "Micellar solutions in contraction slit-flow: alignment mapped by SANS," Journal of Non-Newtonian Fluid Mechanics 2015;215:8–18.

[43] Kalus, J., Hoffman, H. "Nearest neighbor order in an aligned solution of interacting rod-like micelles," The Journal of Chemical Physics 1987;87(1):714–722.

[44] Kalus, J., Chen, S., Hoffmann, H., Neubauer, G., Lindner, P., Thurn, H. "Transient SANS studies of rodlike micelles on a time scale of 100 ms," Journal of Applied Crystallography 1988;21(6):777–780.

[45] Jindal, V., Kalus, J., Pilsl, H., Hoffmann, H., Lindner, P. "Dynamic small-angle neutron scattering study of rodlike micelles in a surfactant solution," Journal of Physical Chemistry 1990;94(7):3129–3138.

[46] Kalus, J., Schmelzer, U. "Small angle neutron (SANS) and x-ray (SAXS) scattering on micellar systems," Physica Scripta 1993;1993(T49B):629.

[47] Butler, P., Magid, L., Hamilton, W., Hayter, J., Hammouda, B., Kreke, P. "Kinetics of alignment and decay in a highly entangled transient threadlike micellar network studied by small-angle neutron scattering," The Journal of Physical Chemistry 1996;100(2):442–445.

[48] Cummins, P.G., Staples, E., Hayter, J.B., Penfold, J. "A small-angle neutron scattering investigation of rod-like micelles aligned by shear flow," Journal of the Chemical Society, Faraday Transactions 1 1987;83(9):2773–2786.

[49] Cummins, P., Staples, E., Penfold, J., Heenan, R. "The geometry of micelles of the poly(oxyethylene) nonionic surfactants C16E6 and C16E8 in the presence of electrolyte," Langmuir 1989;5(5):1195–1199.

[50] Penfold, J., Staples, E., Cummins, P. "Small angle neutron scattering investigation of rodlike micelles aligned by shear flow," Advances in Colloid and Interface Science 1991;34:451–476.

[51] Schmitt, V., Lequeux, F., Pousse, A., Roux, D. "Flow behavior and shear induced transition near an isotropic/nematic transition in equilibrium polymers," Langmuir 1994;10(3):955–961.

[52] Penfold, J., Staples, E., Tucker, I., Cummins, P. "The structure of nonionic micelles in less polar solvents," Journal of Colloid and Interface Science 1997;185(2):424–431.

[53] Nakamura, K., Shikata, T. "Formation and physicochemical features of hybrid threadlike micelles in aqueous solution," ChemPhysChem 2007;8(18):2568–2574.

[54] Takeda, M., Kusano, T., Matsunaga, T., Endo, H., Shibayama, M., Shikata, T. "Rheo-SANS studies on shear-thickening/thinning in aqueous rodlike micellar solutions," Langmuir 2011;27(5):1731–1738.

[55] Rogers, S., Kohlbrecher, J., Lettinga, M. "The molecular origin of stress generation in worm-like micelles, using a rheo-SANS LAOS approach," Soft Matter 2012;8(30):7831–7839.

[56] Walker, L.M., Wagner, N.J. "SANS analysis of the molecular order in poly (γ-benzyl l-glutamate)/deuterated dimethylformamide (PBLG/d-DMF) under shear and during relaxation," Macromolecules 1996;29(6):2298–2301.

[57] Dehmoune, J., Decruppe, J., Greffier, O., Xu, H., Lindner, P. "Shear thickening in three surfactants of the alkyl family CnTAB: Small angle neutron scattering and rheological study," Langmuir 2009;25(13):7271–7278.

[58] Fuller, G.G. Optical Rheometry of Complex Fluids Oxford University Press; 1995.

[59] Berret, J.F., Gamez-Corrales, R., Séréro, Y., Molino, F., Lindner, P. "Shear-induced micellar growth in dilute surfactant solutions," Europhysics Letters 2001;54(5):605.

[60] Truong, M., Walker, L. "Controlling the shear-induced structural transition of rodlike micelles using nonionic polymer," Langmuir 2000;16(21):7991–7998.

[61] Förster, S., Konrad, M., Lindner, P. "Shear thinning and orientational ordering of wormlike micelles," Physical Review Letters 2005;94(1):017803.

[62] Cappelaere, E., Berret, J., Decruppe, J., Cressely, R., Lindner, P. "Rheology, birefringence, and small-angle neutron scattering in a charged micellar system: Evidence of a shear-induced phase transition," Physical Review E 1997;56(2):1869.

[63] Helgeson, M.E., Porcar, L., Lopez-Barron, C., Wagner, N.J. "Direct observation of flow-concentration coupling in a shear-banding fluid," Physical Review Letters 2010;105(8):084501.

[64] Helgeson, M.E., Wagner, N.J., Porcar, L. "Neutron transmission measurements of concentration profiles in non-homogeneous shear flows," NIST Center for Neutron Research: Accomplishments and Opportunities 2010;:38–39.

[65] Berret, J.F., Roux, D., Porte, G., Lindner, P. "Shear-induced isotropic-to-nematic phase transition in equilibrium polymers," Europhysics Letters 1994;25(7):521.

[66] Roux, D.C., Berret, J.F., Porte, G., Peuvrel-Disdier, E., Lindner, P. "Shear-induced orientations and textures of nematic living polymers," Macromolecules 1995;28(5):1681–1687.

[67] Berret, J.F., Roux, D., Porte, G., Lindner, P. "Tumbling behaviour of nematic worm-like micelles under shear flow," Europhysics Letters 1995;32(2):137.

[68] Berret, J.F., Roux, D., Lindner, P. "Structure and rheology of concentrated wormlike micelles at the shear-induced isotropic-to-nematic transition," The European Physical Journal B 1998;5(1):67–77.

[69] Truong, M., Walker, L. "Quantifying the importance of micellar microstructure and electrostatic interactions on the shear-induced structural transition of cylindrical micelles," Langmuir 2002;18(6):2024–2031.

[70] Berret, J.F., Gamez-Corrales, R., Oberdisse, J., Walker, L., Lindner, P. "Flow-structure relationship of shear-thickening surfactant solutions," Europhysics Letters 1998;41(6):677.

[71] Calabrese, M.A., Wagner, N.J., Rogers, S.A. "An optimized protocol for the analysis of time-resolved elastic scattering experiments," Soft Matter (accepted) 2016;.

[72] Liberatore, M.W., Nettesheim, F., Vasquez, P.A., Helgeson, M.E., Wagner, N.J., Kaler, E.W., et al. "Microstructure and shear rheology of entangled wormlike micelles in solution," Journal of Rheology 2009;53(2):441–458.

[73] Croce, V., Cosgrove, T., Dreiss, C.A., King, S., Maitland, G., Hughes, T. "Giant micellar worms under shear: a rheological study using SANS," Langmuir 2005;21(15):6762–6768.

[74] Kalus, J., Hoffmann, H., Ibel, K. "Small-angle neutron scattering on shear-induced micellar structures," Colloid and Polymer Science 1989;267(9):818–824.

[75] Münch, C., Hoffmann, H., Ibel, K., Kalus, J., Neubauer, G., Schmelzer, U., et al. "Transient small-angle neutron scattering experiments on micellar solutions with a shear-induced structural transition," The Journal of Physical Chemistry 1993;97(17):4514–4522.

[76] Oda, R., Weber, V., Lindner, P., Pine, D., Mendes, E., Schosseler, F. "Time-resolved small-angle neutron scattering study of shear-thickening surfactant solutions after the cessation of flow," Langmuir 2000;16(11):4859–4863.

[77] Lin, M., Hanley, H., Straty, G., Peiffer, D., Kim, M., Sinha, S. "A small-angle neutron scattering (SANS) study of worm-like micelles under shear," International Journal of Thermophysics 1994;15(6):1169–1178.

[78] Lin, M., Hanley, H., Sinha, S., Straty, G., Peiffer, D., Kim, M. "A small angle neutron scattering study of worm-like micelles," Physica B: Condensed Matter 1995;213:613–615.

[79] Lin, M., Hanley, H., Sinha, S., Straty, G., Peiffer, D., Kim, M. "Shear-induced behavior in a solution of cylindrical micelles," Physical Review E 1996;53(5):R4302.

[80] Kalus, J., Hoffmann, H., Chen, S., Lindner, P. "Correlations in micellar solutions under shear: A small-angle neutron scattering study of the chain surfactant n-hexadecyloctyldimethylammonium bromide," The Journal of Physical Chemistry 1989;93(10):4267–4276.

[81] Schmitt, V., Schosseler, F., Lequeux, F. "Structure of salt-free wormlike micelles: signature by SANS at rest and under shear," Europhysics Letters 1995;30(1):31.

[82] Cummins, P., Hayter, J., Penfold, J., Staples, E. "A small-angle neutron scattering investigation of shear-aligned hexaethyleneglycolmonohexadecylether (C16E6) micelles as a function of temperature," Chemical Physics Letters 1987;138(5):436–440.

[83] Lonetti, B., Kohlbrecher, J., Willner, L., Dhont, J., Lettinga, M. "Dynamic response of block copolymer wormlike micelles to shear flow," Journal of Physics: Condensed Matter 2008;20(40):404207.

[84] Qi, Y., Littrell, K., Thiyagarajan, P., Talmon, Y., Schmidt, J., Lin, Z., et al. "Small-angle neutron scattering study of shearing effects on drag-reducing surfactant solutions," Journal of Colloid and Interface Science 2009;337(1):218–226.

[85] Angelico, R., Olsson, U., Mortensen, K., Ambrosone, L., Palazzo, G., Ceglie, A. "Relaxation of shear-aligned wormlike micelles," The Journal of Physical Chemistry B 2002;106(10):2426–2428.

[86] Angelico, R., Rossi, C.O., Ambrosone, L., Palazzo, G., Mortensen, K., Olsson, U. "Ordering fluctuations in a shear-banding wormlike micellar system," Physical Chemistry Chemical Physics 2010;12(31):8856–8862.

[87] Kline, S.R. "Reduction and analysis of SANS and USANS data using IGOR Pro," Journal of Applied Crystallography 2006;39(6):895–900.

[88] Spenley, N., Yuan, X., Cates, M. "Nonmonotonic constitutive laws and the formation of shear-banded flows," Journal de Physique II 1996;6(4):551–571.

[89] Fielding, S.M. "Complex dynamics of shear banded flows," Soft Matter 2007;3(10):1262–1279.

[90] Olmsted, P.D. "Perspectives on shear banding in complex fluids," Rheologica Acta 2008;47(3):283–300.

[91] Adams, J., Olmsted, P. "Nonmonotonic models are not necessary to obtain shear banding phenomena in entangled polymer solutions," Physical Review Letters 2009;102:067801.

[92] Manneville, S. "Recent experimental probes of shear banding," Rheologica Acta 2008;47(3):301–318.

[93] Mair, R., Callaghan, P. "Observation of shear banding in worm-like micelles by NMR velocity imaging," Europhysics Letters 1996;36(9):719.

[94] Britton, M.M., Callaghan, P.T. "Two-phase shear band structures at uniform stress," Physical Review Letters 1997;78(26):4930.

[95] Hu, Y., Lips, A. "Kinetics and mechanism of shear banding in an entangled micellar solution," Journal of Rheology 2005;49(5):1001–1027.

[96] Hu, Y., Palla, C., Lips, A. "Comparison between shear banding and shear thinning in entangled micellar solutions," Journal of Rheology 2008;52(2):379–400.

[97] Thareja, P., Hoffmann, I.H., Liberatore, M.W., Helgeson, M.E., Hu, Y.T., Gradzielski, M., et al. "Shear-induced phase separation (SIPS) with shear banding in solutions of cationic surfactant and salt," Journal of Rheology 2011;55(6):1375–1397.

[98] Berret, J.F. "Transient rheology of wormlike micelles," Langmuir 1997;13(8):2227–2234.

[99] Sachsenheimer, D., Oelschlaeger, C., Müller, S., Küstner, J., Bindgen, S., Willenbacher, N. "Elongational deformation of wormlike micellar solutions," Journal of Rheology 2014;58(6):2017–2042.

[100] Candau, S., Oda, R. "Linear viscoelasticity of salt-free wormlike micellar solutions," Colloids and Surfaces A: Physicochemical and Engineering Aspects 2001;183:5–14.

[101] Ziserman, L., Abezgauz, L., Ramon, O., Raghavan, S.R., Danino, D. "Origins of the viscosity peak in wormlike micellar solutions. 1. mixed catanionic surfactants. a cryo-transmission electron microscopy study," Langmuir 2009;25(18):10483–10489.

[102] Fielding, S.M., Olmsted, P.D. "Flow phase diagrams for concentration-coupled shear banding," The European Physical Journal E 2003;11(1):65–83.

[103] Hyun, K., Wilhelm, M., Klein, C.O., Cho, K.S., Nam, J.G., Ahn, K.H., et al. "A review of nonlinear oscillatory shear tests: Analysis and application of large amplitude oscillatory shear (LAOS)," Progress in Polymer Science 2011;36(12):1697–1753.

[104] Rogers, S.A. "A sequence of physical processes determined and quantified in LAOS: An instantaneous local 2d/3d approach," Journal of Rheology 2012;56(5):1129–1151.

[105] Zhou, L., Cook, L.P., McKinley, G.H. "Probing shear-banding transitions of the VCM model for entangled wormlike micellar solutions using large amplitude oscillatory shear (LAOS) deformations," Journal of Non-Newtonian Fluid Mechanics 2010;165(21):1462–1472.

[106] Stickel, J.J., Knutsen, J.S., Liberatore, M.W. "Response of elastoviscoplastic materials to large amplitude oscillatory shear flow in the parallel-plate and cylindrical-Couette geometries," Journal of Rheology 2013;57(6):1569–1596.

[107] Fardin, M.A., Perge, C., Casanellas, L., Hollis, T., Taberlet, N., Ortín, J., et al. "Flow instabilities in large amplitude oscillatory shear: a cautionary tale," Rheologica Acta 2014a;53(12):885–898.

[108] Tapadia, P., Ravindranath, S., Wang, S.Q. "Banding in entangled polymer fluids under oscillatory shearing," Physical Review Letters 2006;96(19):196001.

[109] Ravindranath, S., Wang, S.Q. "Large amplitude oscillatory shear behavior of entangled polymer solutions: Particle tracking velocimetric investigation," Journal of Rheology 2008;52(2):341–358.

[110] Li, X., Wang, S.Q., Wang, X. "Nonlinearity in large amplitude oscillatory shear (LAOS) of different viscoelastic materials," Journal of Rheology 2009;53(5):1255–1274.

[111] Dimitriou, C.J., Casanellas, L., Ober, T.J., McKinley, G.H. "Rheo-PIV of a shear-banding wormlike micellar solution under large amplitude oscillatory shear," Rheologica Acta 2012;51(5):395–411.

[112] Germann, N., Gurnon, A.K., Zhou, L., Cook, L.P., Beris, A.N., Wagner, N.J. "Validation of constitutive modeling of shear banding, threadlike wormlike micellar fluids," submitted to Journal of Rheology 2016;.